Experimental Measurements of Heat Transfer from a Cylinder to Turbulent Isothermal and Non-Isothermal Jets

Karthik Balasubramanian

Thesis submitted to the faculty of the Virginia Polytechnic Institute and State University in partial fulfillment of the requirements for the degree of

Master of Science

In

Mechanical Engineering

Thomas E. Diller, Chair

Scott T. Huxtable

Rui Qiao

04/28/2016
Blacksburg, Virginia

Keywords: Isothermal jets, Frossling number, Froude number, Heat transfer

Experimental Measurements of Heat Transfer from a Cylinder to Turbulent Isothermal and Non-Isothermal Jets

Karthik Balasubramanian

ABSTRACT

This work is an experimental study of the effect of impinging distance on the heat transfer from a cylinder to turbulent isothermal and non-isothermal jets. The isothermal jet is discharged horizontally at the same temperature as the ambient air while the non-isothermal jet is discharged vertically upwards and vertically downwards at a temperature colder than the ambient air. Temperature measurements are made on a heated cylinder using an infrared (IR) camera at five equal impinging distances ranging from Z/d =4 to Z/d=20 and the distributions of the local Frossling numbers are determined. The overall decrease in the average Frossling numbers of the cylinder impinged by the isothermal jet and the cold jets was 25 % and 40% respectively. The peak values of average Frossling number for the isothermal and the cold jets occurred at Z/d=8 and Z/d=4 respectively. The Stagnation Frossling number and the normalized jet centerline velocity for the isothermal and the cold jets were found to be very close to each other at all impinging distances indicating that the effect of buoyancy is negligible in the range of jet temperatures and distances used in the experiment.

Experimental Measurements of Heat Transfer from a Cylinder to Turbulent Isothermal and Non-Isothermal Jets

Karthik Balasubramanian

GENERAL ABSTRACT

Impingement jets are used in a wide range of applications such as gas turbine cooling, electronics cooling and annealing of metals because they provide high convective heat transfer rates. The current work is aimed at evaluating the heat transfer characteristics of impingement jets which could also be used in the microenvironment conditioning of a building space. Microenvironment conditioning refers to the process in which the thermal conditions of a small zone in the building are individually controlled by its occupants. The advantages of this process is that it caters to the thermal comforts of each individual occupant and reduces the overall energy consumption in a building when compared to conventional heating or cooling methods. In the current study, the heat transfer from a human arm in a thermally conditioned microenvironment is experimentally simulated by a heated cylinder impinged by a turbulent jet. The distance between the cylinder and the origin of the jet is varied and its effect on the overall heat transfer is studied. An infrared camera is used to record the temperature distribution around the heated cylinder which is then used to compute the overall heat transfer. The experimental results show that the jets provide substantial heat transfer rates even at large impinging distances. Thus the impinging jets can be considered an effective means of creating thermally conditioned microenvironments.

Dedication

This work is dedicated to my family whose unwavering love and encouragement has kept me motivated at all times

Acknowledgments

I would sincerely like to thank everybody who have supported me in various forms throughout my Master's program. First and Foremost, I would like to express my deepest gratitude to my advisor, Dr. Diller for providing me the opportunity to be a part of his research group and guiding me at every stage of my research. His wealth of knowledge and experience has strengthened my engineering fundamentals and has helped me become a more rounded engineer. I am certain that some of the skills I have learnt from him would be extremely beneficial at many stages of my career. I would also like to thank Dr. Huxtable and Dr. Qiao for their guidance and willingness to be a part of my committee.

Next, I would like to thank all my lab mates, Chris, Rande, Abdul, Ali, Tim and Ryan for their assistance and support. The constant banter and jovial atmosphere in the lab kept me lighthearted at all times and I thoroughly enjoyed my time working with them in the Heat Transfer Measurements Lab.

Last but not least, I would like to acknowledge my family and friends for all their help and encouragement.

Table of Contents

List of Figures

List of Tables

Nomenclature

A_s	Surface Area (m^2)
d	Diameter of the jet at origin(m)
D	Diameter of the cylinder (m)
Fr	Froude number
Fro	Frossling number
g	Acceleration due to gravity (m/s^2)
h	Heat transfer coefficient (W/m^2-K)
IR	Infrared
k	Thermal conductivity(W/m-K)
Nu	Nusselt number
ΔP	Differential pressure (Pa)
q"	Heat flux(W/m^2)
q_{total}	Total heat transfer (W)
R	Resistance (Ω)
R_a	Gas constant of air (kJ/kg-K)
Re_d	Reynolds number based on jet diameter
Re_D	Reynolds number based on cylinder diameter
s	Distance along cylinder axis (m)
T	Temperature (˚C)
ΔT	Temperature difference with respect to ambient (˚C)
U	Centerline velocity (m/s)
V	Voltage (V)
Z	Impinging Distance from jet origin(m)

Greek

β	Coefficient of expansion (1/K)
ε	Emissivity
ρ	Density (kg/m^3)
μ	Dynamic viscosity (kg/m-s)
θ	Circumferential angle (degree)
σ	Stefan-Boltzmann Constant ($5.67x10^{-14}W/m^2$-K^4)

Subscripts

0	Jet exit properties
j	Impinging properties of jet
∞	Ambient fluid properties
avg	Average values
stag	Stagnation point values
iso	Isothermal jet properties
conv	Convected heat flux
local	Local values at cylinder surface

Chapter 1. Thesis Organization

The Thesis is organized into five chapters. Chapter 2 provides an introduction into some of the fundamental concepts that govern the flow characteristics of isothermal and vertical non-isothermal jets and summarizes previous research that has helped in understanding some of the main factors that influence heat transfer of a cylinder impinged by a turbulent jet. Chapter 3 contains a detailed explanation about the experimental set up and the data reduction process. Chapter 4 describes the experimental results that is used for the comparison of the velocity and heat transfer characteristics of the isothermal and the two cold jets. Chapter 5 summarizes some of the main findings of the experiments and contains recommendations that would aid in broadening the scope of the current study. Appendix A contains plots of the variation of jet exit temperature based Frossling numbers with distance. Appendix B contains the uncertainty calculations for various measured parameters. Appendix C contains the experimental procedure followed to quantify the IR camera viewing angle and Appendix D describes the IR camera emissivity correction procedure.

Chapter 2: Introduction

Impingement jets are used in a wide range of applications because they provide high convective heat transfer rates. Some of these applications include cooling of gas turbines, electronics cooling, annealing of metals and ventilation of buildings. This work aims to study the heat transfer characteristics of an impinging jet used in the microenvironment conditioning of a building. Microenvironment conditioning refers to the process where the thermal conditions of a small zone or space in a building are individually controlled by its occupants [1]. The main advantages of such a system is that it caters to the comforts of all individuals and provides substantial energy savings compared to traditional methods where the entire building space is conditioned. Most of the commercially microenvironment units are either floor mounted or desk-mounted [1,2] and use individual supply fans or radiant heaters for providing thermal comfort.

The current study aims to quantify the heat transfer characteristics of a turbulent jet of diameter d impinging on a heated cylinder (Diameter denoted by D), to mimic the heat transfer of a human arm in a micro environment thermally conditioned by the impinging jet. Although many numerical and experimental heat transfer studies have been performed for turbulent jets impinging on large cylinders($D/d>5$), very little literature is available for heat transfer in smaller cylinders. In the experiments used in this work, a cylinder of curvature ratio $D/d=0.6$ is impinged by an isothermal, vertically upward and downward cold jet discharged with high Reynolds numbers at five impinging distances.

A submerged Isothermal jet is the discharge of a stream of fluid into a static surrounding fluid that is at the same temperature as the discharged fluid. The jet is called a free jet if it does not interact with any medium other than the surrounding fluid. Extensive numerical and experimental work has been done to understand the centerline and radial distributions of velocity of a free and impinging round isothermal jet. The following sections discuss some of the velocity characteristics of these jets.

2.1 Free Isothermal Jets

There are three main regions that explain the velocity profiles in the cross-section a free jet[3]; the initial region, a transition region and a fully developed or the main region as illustrated in Fig. 1. In the initial region as the jet exits the mouth of nozzle or the orifice, the velocity is constant after which the jet begins interacting with the surrounding static fluid causing the formation of a shear

layer. Along the jet axis, the viscous effect of the static fluid causes thickening of the shear layer thereby forcing the jet velocity near the jet-static fluid boundary to slow down. However, these effects do not impact the core velocity of the jet up to a certain axial distance from the jet exit.

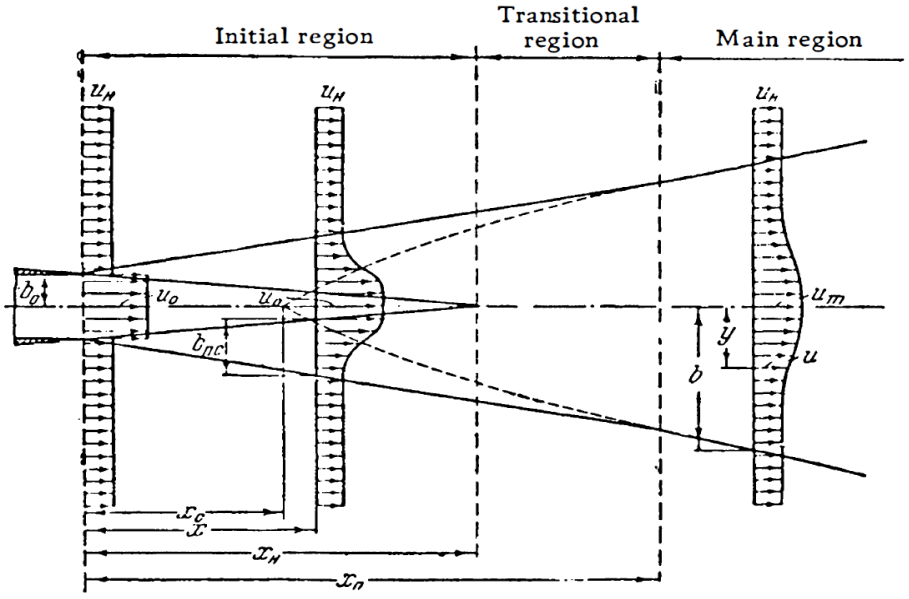

Figure 1: Regions of A free Jet[3], Abramovich G.N,Schindel L.,The Theory of Turbulent Jets, MIT press,2003,Used under fair use,2016

The axial distance from the jet axis up to which the centerline velocity of the jet remains constant is known as the potential core length. However, the value of the potential core length is highly dependent on the nozzle geometry [4]. Beyond the potential core, the centerline velocity of the jet begins to drop and the velocity profiles at the cross-section keep varying in the transition region. At the end of the transition region the velocity profile across the cross-section is fully developed and resembles a Gaussian distribution for all impinging distances further downstream [5]. The rate at which the centerline velocity decays in the fully developed region is inversely proportional to the distance ratio from the jet exit and can be expressed as

$$\frac{U_j}{U_0} = \frac{\text{Constant}}{(Z/d)} \qquad (1)$$

Where U_j is the centerline velocity of the free jet at a distance Z from its origin and U_0 is the centerline velocity of the jet at the origin

2.2 Impinging Isothermal Jet

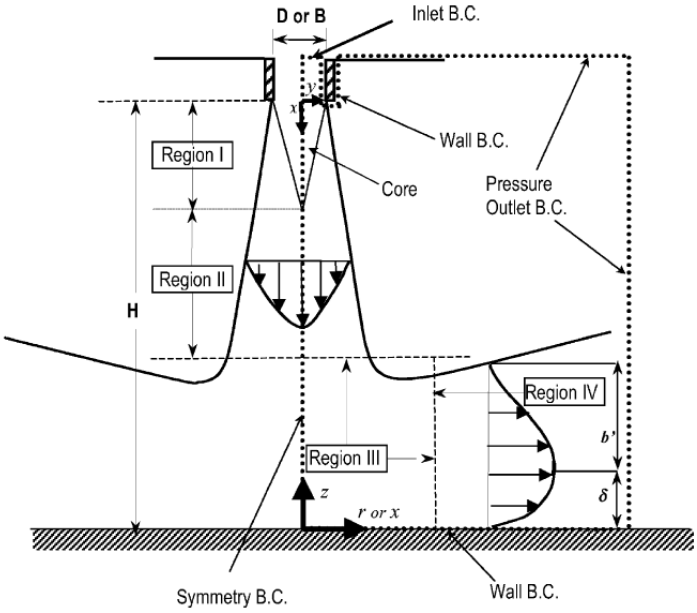

Figure 2: Regions of an Impinging Jet [6], Coussirat, M., Van Beeck, J., Mestres, M., Egusguiza, E., Buchlin, J.-M., and Escaler, X., 2005, "Computational Fluid Dynamics Modeling of Impinging Gas-Jet Systems: I. Assessment of Eddy Viscosity Models," J. Fluids Eng., 127(4), p. 691. Used under fair use,2016

The velocity characteristics of a jet impinging on a target surface is somewhat different to that of a free jet. The velocity profiles in an impinging jet are not only governed by the jet exit Reynolds number and nozzle geometry but also the distance of the target surface from the jet. In case of vertical impinging jets, at some distance upstream of the target surface the vertical velocity of the jet decreases rapidly and is gradually transformed into a horizontal component [5]. This region is often referred to as the stagnation region of the jet [7]. Giralt et al. [8] characterized the length of this region to be about 1.2 times the nozzle diameter from the stagnation point. At the stagnation point the velocity of the jet is zero while the static pressure is highest. The region of the flow beyond the stagnation point is called the wall jet region (marked as Region 4 in Fig.2). In this region the flow accelerates as it moves some distance along the surface due to a favorable pressure gradient and the velocity profile is asymmetric as the flow is bounded by the target surface on one side and by the surrounding fluid on the other side as shown in Fig. 2.

2.3 Background of Heat Transfer Measurements of Isothermal Jets

The review on circular jet impingement by Jambunathan et al. [7] lists Reynolds number, turbulence intensity, impinging distance and nozzle geometry as some of the main factors affecting heat transfer from cylindrical surfaces to impinging jets. Cornaro et al.[9] investigated the circumferential Nusselt distribution for cylinders with D/d values of 2.63 to 5.55 over a wide range of jet diameter based Reynolds number(Re_d) of 6000-16000. They concluded that at low Reynolds number, the value of D/d has a negligible effect on the local Nusselt number distribution, while at higher Reynolds numbers the curvature effect has a significant effect. Wang et al.[10] investigated the heat transfer characteristics of cylinders over a wide range of surface curvatures (D/d =5,1,0.5) at a fixed Reynolds number (Re_d) of 20000. They concluded that the heat transfer characteristics of the smaller cylinder (D/d= 0.5) is similar to one that is immersed in a uniform stream while those of the larger cylinders (D/d= 1,5) resemble a flat plate being impinged by a circular jet. Gori et al.[11] investigated the effect of Reynolds number on the Nusselt number distribution on the surface of a cylinder used a slot jet with a slot height to jet diameter ratio of 2. Their findings showed that the location of the minimum local Nusselt along the cylinder circumference varies at different Reynolds number and impinging distances.

Gardon and Akfirat [12] studied the effect of turbulence on the heat transfer characteristics of both slot and circular free jets. They reported that for Reynolds numbers greater than 2750, the axial turbulence intensity continuously increases up to an impinging distance of Z/d=8 even though the center line velocity starts to decay at a distance of Z/d=5. They attributed increasing turbulence to the entrainment effects of the ambient fluid and suggested that this causes the stagnation point heat transfer to increase even at impingement distances beyond the potential core. Their results agreed with that of Lee et al. [13]. who performed heat transfer measurements on round jets impinging on cylindrical surfaces over a wide range of Reynolds numbers. Their study showed that the stagnation Nusselt number reached a maximum at an impinging distance of approximately Z/d=6-8 for cylinders with varying D/d ratios across all Reynolds number.

2.4 Vertical Non-Isothermal Jets

A non-isothermal jet is the discharge of the stream of fluid into a surrounding fluid which is at a different temperature compared to the discharged fluid. If the temperature variation of the surrounding fluid in the direction of the jet axis is negligible then it is known as a uniform environment while a stratified environment is one where the temperature of the surrounding fluid changes in the direction of the jet axis. In addition to the inertial force near the origin, the jet experiences a buoyant force due to the difference in temperature (or density) between the jet and the environment. When this temperature difference is high, the buoyancy effects dominate over the inertial effects at large distances from the jet exit and such non-isothermal jets are also known as buoyant jets. The Buoyant jets are classified as positive and negative depending on the direction of buoyancy force with respect to jet velocity at the origin. When the buoyancy force acts in the same direction as the jet exit velocity it is known as a positive buoyant jet and when the buoyancy force acts in a direction opposite to that of the jet exit velocity then it is known as a negative buoyant jet[14]. Consequently, a heated jet discharged vertically upwards or a cooled jet discharged vertically downwards are examples of positive buoyant jets while a heated jet discharged vertically downwards and a cooled jet discharged vertically upwards are examples of negative buoyant jets.

There are three main regions in any free vertical buoyant jet; the non-buoyant region, transition region and the plume or the buoyant region. The region near the jet origin is the non-buoyant region in which the inertial forces are significantly higher than the buoyancy forces and hence the jet behaves like an isothermal jet[14]. In the transition region of the jet, the inertial effects begin to decline as the jet moves further downstream from the origin. In the final region, the influence of the inertial forces is completely diminished and the flow is now solely governed by the buoyancy forces. In this region, the direction of fluid flow remains unaltered for a positive buoyant jet whereas a flow reversal occurs for a negative buoyant jet as shown in Fig. 3.

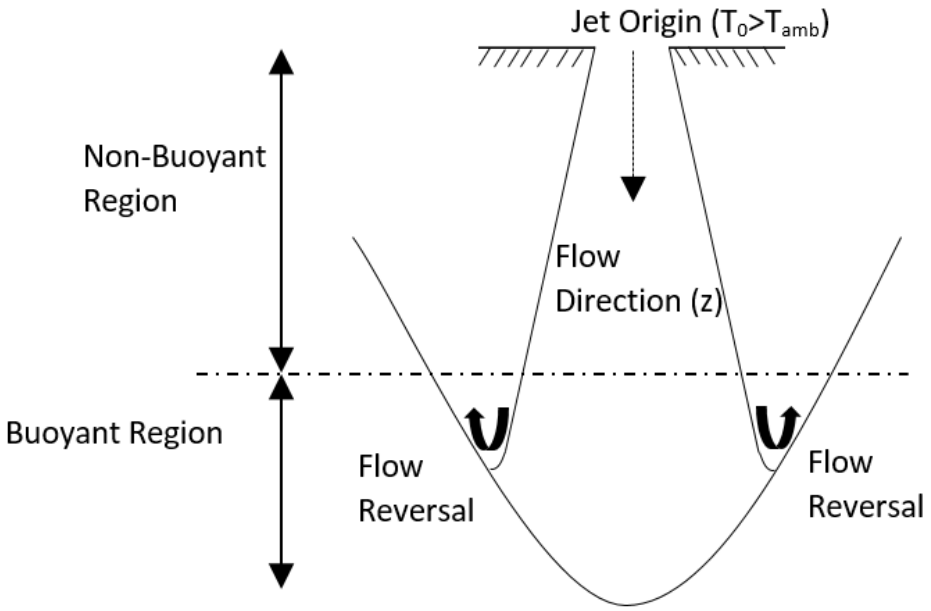

Figure 3: Flow reversal in a negative Buoyant Jet

2.5 Empirical Correlations for Velocity and Temperature of Buoyant Jets

Ogino et al.[15] developed empirical correlations that describe the velocity and temperature characteristics of a heated jet discharged vertically upwards in uniform environment over a wide range of Froude numbers (16-33200). The following correlations describe the lengths of the three regions of the positive buoyant jet

I. Non-buoyant region $0.1 \leq \frac{Z}{d\sqrt{Fr}} \leq 1$

II. Transition region $1 \leq \frac{Z}{d\sqrt{Fr}} \leq 1$

III. Buoyant region $5 < \frac{Z}{d\sqrt{Fr}}$

where, Fr is the Froude number at the exit of the jet and is given by the expression

$$Fr = \frac{U_0^2}{g\beta(T_0 - T_\infty)d} \quad (2)$$

The Froude number represents the ratio of the inertial effects to the buoyancy effects of the jet. The following correlations are applicable for the decay of centerline velocity along the jet axis:

$$\sqrt{Fr}\,\frac{U_j}{U_o} = 5.8\left(\frac{Z}{d\sqrt{Fr}}\right)^{-1} \quad \text{in the Non-buoyant region} \tag{3}$$

$$\sqrt{Fr}\,\frac{U_j}{U_o} = 5.8\left(\frac{Z}{d\sqrt{Fr}}\right)^{-2/3} \quad \text{in the Transition region} \tag{4}$$

$$\sqrt{Fr}\,\frac{U_j}{U_o} = 3.4\left(\frac{Z}{d\sqrt{Fr}}\right)^{-1/3} \quad \text{in the Buoyant region} \tag{5}$$

In the same study the correlations for the decay of centerline temperature are given by the expressions:

$$\sqrt{Fr}\,\frac{(T_j - T_o)}{(T_o - T_\infty)} = 4.8\left(\frac{Z}{d\sqrt{Fr}}\right)^{-1} \quad \text{in the non-buoyant region} \tag{6}$$

$$\sqrt{Fr}\,\frac{(T_j - T_o)}{(T_o - T_\infty)} = 4.8\left(\frac{Z}{d\sqrt{Fr}}\right)^{-5/4} \quad \text{in the transition region} \tag{7}$$

$$\sqrt{Fr}\,\frac{(T_j - T_o)}{(T_o - T_\infty)} = 9.4\left(\frac{Z}{d\sqrt{Fr}}\right)^{-5/3} \quad \text{in the buoyant region} \tag{8}$$

Mizushina et al. [16]developed correlations to quantify the velocity and temperature decay of a heated jet discharged vertically downwards. While the decay of centerline temperature was in in agreement with Ogino's results, there was a slight downward deviation of center line velocity decay especially near the end of the non-buoyant region.

2.6 Background of Heat transfer measurement techniques

Various researchers have used a variety of techniques for measuring heat transfer from impinging jets. The use of single or an array of thermocouples embedded on the target surface is one of the frequently used ways of measuring temperature[10,17,18]. The temperature difference between the surface and the fluid and the convective heat flux measured using a heat flux sensor is then used to compute the local heat transfer coefficient. However, the main drawback of using thermocouples is that the temperature measurements can be carried out only at discrete points and its use is often time consuming for experiments which require spatially resolved temperature data. Sparrow et al.[19]. used the naphthalene sublimation technique in which a cylinder coated with

naphthalene rings was impinged by a circular jet at multiple distances. The decrease in mass of naphthalene due to sublimation is used to estimate the Sherwood number and the heat mass transfer analogy is used to transform the Sherwood number into the corresponding Nusselt number. High accuracy, low losses and well controlled boundary conditions are some of the advantages in using sublimation technique. Liquid Crystal Thermography is another commonly used technique in which the impinged target surface is embedded or coated with liquid crystals that reflect different colors when exposed to white light depending on the temperature of the surface. The change in the lattice structure due to temperature variations enables the liquid crystal to reflect only one component of light while transmitting the remaining components[20]. Each color reflected by the crystal represents a constant temperature contour on the impinged surface and hence are referred to as isotherms. Infrared Thermography is another commonly used technique in heat transfer experiments in which the radiation emitted by the impinged surface is measured and converted to a thermal image by an IR camera. The main advantages of IR thermography over Liquid Crystal Thermography are simpler calibration procedures and lesser sensitive test procedures[21].

In the current study , temperature measurements on the heated cylinder are made using a IR camera at the front and rear portions of the cylinder while the jet temperature measurements are made using a T Type thermocouple.

Chapter 3: Experimental Design and Apparatus

3.1 Experimental Design

The experimental setup shown in Fig. 4 was used for a horizontal turbulent isothermal jet impinging on a heated cylinder at five different distances. The cylinder was heated by a uniform heat flux source and an IR camera was used to the measure the circumferential temperature distribution of the cylinder from θ=0˚ to θ=180˚. Each end of the cylinder was firmly mounted to prevent oscillation or rotation when impinged by the turbulent jet. The heights of mounts were designed to ensure that the cylinder axis was aligned with the axis of the jet.

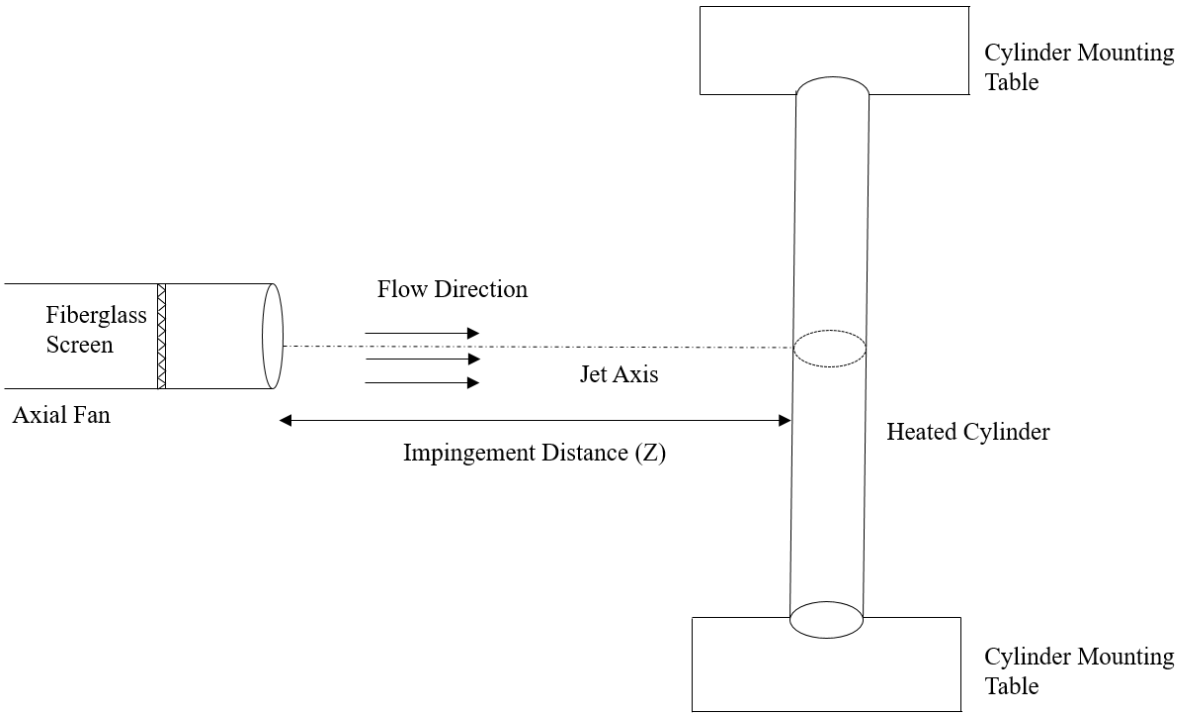

Figure 4: Experimental Setup for the Horizontal Impingement of an Isothermal Jet

Figure 5 shows the experimental setup of a cold jet impinging downwards on the cylinder.

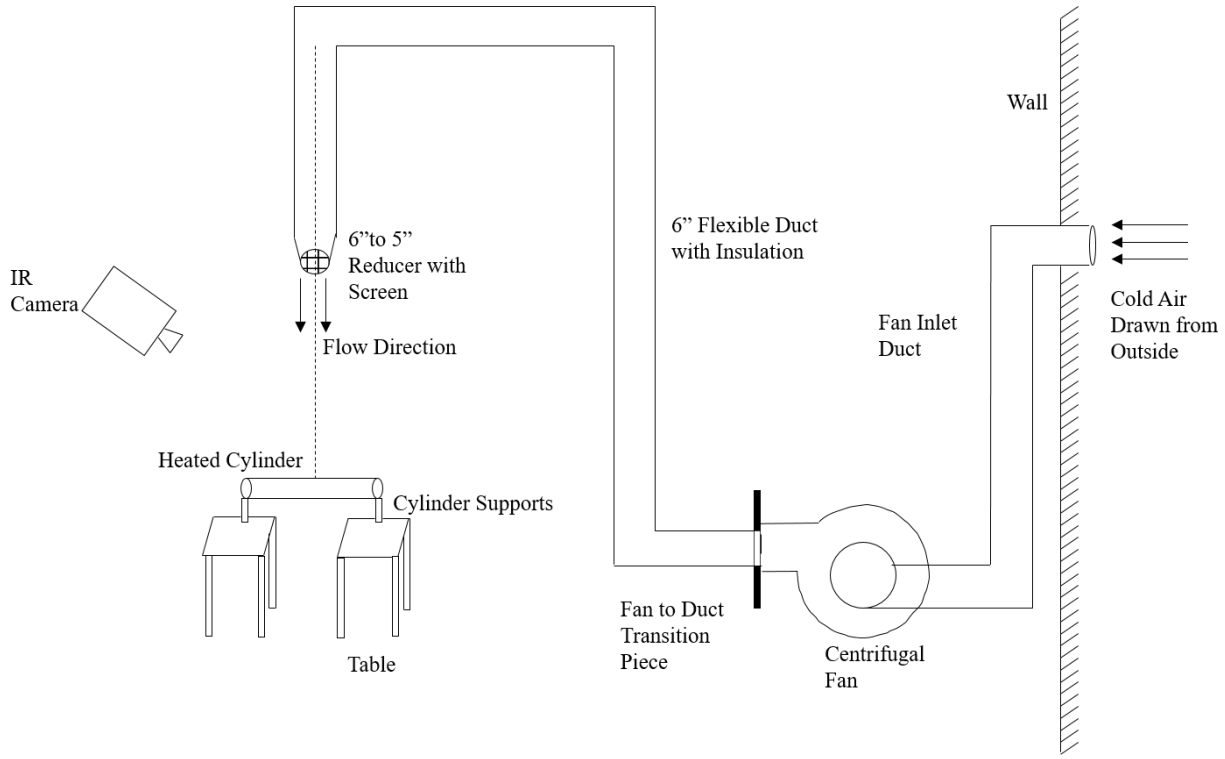

Figure 5: Vertical Non-Isothermal Jet Experimental Setup

3.2 Experimental Apparatus

3.2.1 Axial Fan Wind Tunnel

The turbulent jet for the experiment was created using an axial fan wind tunnel which drew in air at room temperature (24.8˚C). The fan was mounted on a fixed table of height 27" and was powered by a TekPower 30V,10Amp DC Power source. The speed of the fan was kept constant by keeping the input current fixed at 6.5 Amps. The diameter of the wind tunnel was 5.2" and its length was about 66" from the fan to the exit. The center of the wind tunnel was at an elevation of 7.6" inches from the surface of the fixed table. Flow straighteners and a fiberglass screen mesh were placed in the cross-section of the flow at a distance of 33" and 18" upstream from the fan exit respectively. The velocity at the exit of the wind tunnel was measured using a pitot tube connected to a Dwyer Mark II Model 40 differential manometer. The velocity at the exit of the

nozzle was found to be uniform and is used as a reference in all heat transfer calculations for the isothermal jet.

3.2.2 Centrifugal Fan and Duct System

Both upward and downward cold jets were generated using a constant speed centrifugal fan which drew cold air from outside during winter. This was found to be the most convenient way to generate a temperature difference of approximately 10 ˚C or more with respect to room temperature at high volumetric flow rates of the impinging jet. The cold air drawn from outside was supplied to the fan inlet via an insulated duct. The duct and fan connections were sealed to prevent the fan from drawing room temperature air. The outlet of the fan was rectangular in cross-section of dimensions 19.5”x 15” to which a transition piece with a 6” nipple was attached. A 6” round, flexible duct with fiberglass insulation was connected to the nipple and supported from the top using water pipes that ran along the ceiling for the downward discharge of the non-isothermal jet. In case of upward discharge, the duct was kept upright and fastened to a stool using Velcro straps. A 6” to 5” reducer and a fiberglass screen were added to the end of the duct to ensure that the flow was uniform.

3.2.3 Cylinder Construction

The cylinder used in the isothermal experiment measured 3.18” in outer diameter and 10” in length. Two wooden blocks each of height 7.6” were placed at placed on a portable table that had the same elevation from the ground level as the fixed table. The section view of the cylinder in Fig. 6 shows the detailed construction of the heated cylinder. An adhesive backed neoprene rubber sheet of thickness 5/32” was wrapped around a PVC pipe of outside diameter 2.875”. A Minco foil heater of resistance 60 Ω and dimensions 10”x 10” with aluminum backing of thickness 0.005” was wrapped and stuck around the rubber sheet using a thin layer of 3M Rubber and Vinyl Spray adhesive. The aluminum foil ensured a uniform distribution of the flux over the cylindrical surface especially in spaces between the heater elements by means of conduction. A thin layer of Aervoe Z635 Black Zynolyte High Temperature Paint was sprayed over the cylinder and dried under the exhaust hood. In case of the vertical cold jets, instead of the Minco heater, a resistance heater of resistance 56 Ω and dimensions of 10”x8” was screen printed in the Heat Transfer Measurement Lab. The same core materials, adhesive and black paint as the previous case were used to construct the cylinder.

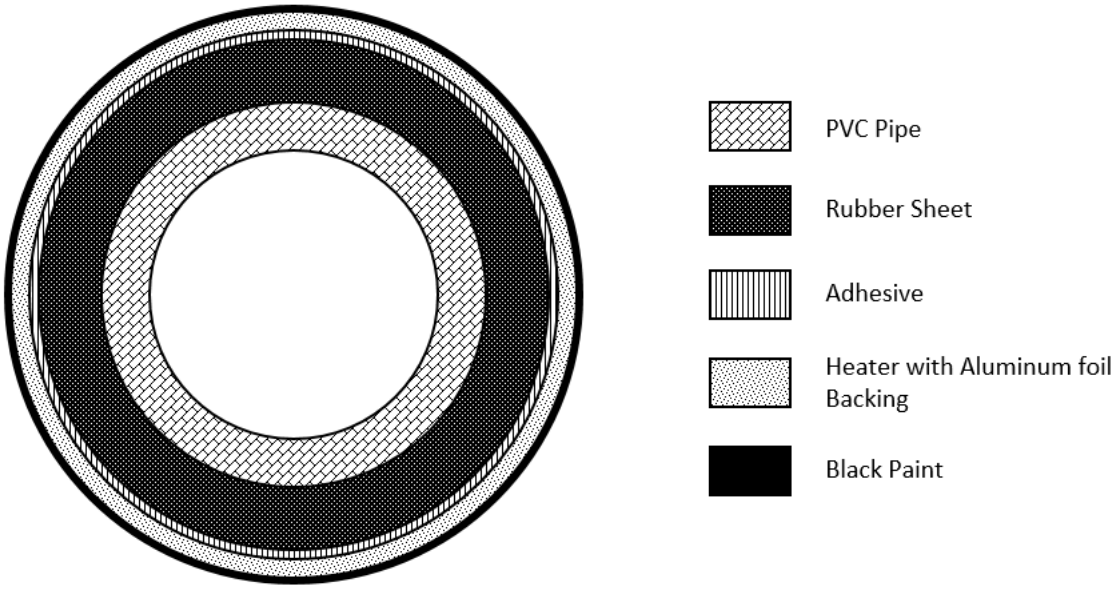

Figure 6: Section View of The Cylinder (Not Drawn to scale)

3.2.4 Power Source

The lead wires of both the heaters were connected to a Model SC-10 T AC Variac with a maximum power rating of 2kW. The voltage was set to an RMS voltage of 60 V and 61.5 V for the isothermal and the cold jets respectively and was measured using a HP 3468 true RMS Multimeter. The resistance of the heater was also measured using the Multimeter and the total current drawn by the circuit was calculated using Ohms law.

3.2.5 IR Camera

The temperature measurements of the surface of the heated cylinder were made using a FLIR A655SC IR Camera. The camera had a resolution of 640x480 pixels and had a temperature measurement range of -40˚C to 150˚C with an accuracy of $\pm$2˚C. The IR camera was connected to a laptop via a Gigabit Ethernet Cable and data was acquired and processed using the FLIR TOOLS software. In the isothermal jet experiment, the IR camera was fixed to an articulating arm via three M4 screws while for the cold jets it was mounted on a tripod.

Since the emissivity of the black paint on the cylinder surface was unknown, the IR camera was calibrated against a T type thermocouple welded on a flat plate sprayed with the same paint. The details about the IR camera calibration procedure are explained in Appendix D. The emissivity of the black paint was found to 0.94 and was in good agreement with previously measured values[22].

While using an IR camera to perform temperature measurements on a curved surface such as a cylinder, it is important to take into account the errors in measurements due to changes in directional emissivity along the surface curvature. The degree of temperature variations on the surface is dependent upon the angle between direction of emission and the normal to surface, referred to as the viewing angle [23]. According to previous studies [23,24], viewing angles less than 60˚ have a negligible effect on the temperature measurements on the surface of the cylinder. For the current experiment viewing angles of less than 55˚ yielded a temperature variation of less than 0.1 ˚C on a vertical cylinder under natural convection. The details of the quantification of viewing angle is explained in Appendix B.

In the current experiment, the IR camera was fixed at a viewing angle of 45˚ with respect to the stagnation point (θ=0˚) of the cylinder when viewing the front portion of the cylinder and at 45˚ with respect to θ=180˚ when viewing the rear portion. A 45˚ wooden wedge was used to align and fix the viewing angle on the respective IR mounting devices. Figure 7 shows the position of the IR camera relative to the cylinder

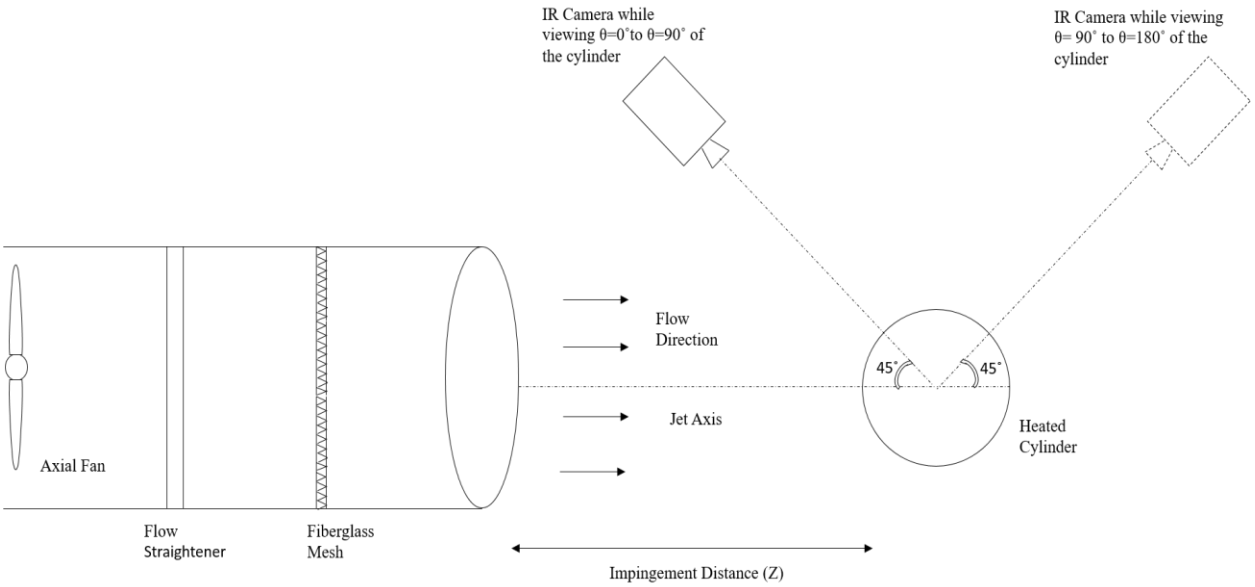

Figure 7: Position of IR Camera Relative to Cylinder

3.2.6 Angle Measurement Grid

In order to measure the angular displacement from the Stagnation point, Colban et al.[25] captured an IR image of a 1x1 cm grid placed on the curved surface and used the grid vortices to perform a third order polynomial transformation to take into account the curvature effect. In this experiment, a sheet paper of width 10 inches (equal to circumference of the cylinder) and height 6 inches was divided into 72 equal rectangular blocks of width 0.138". The height of each rectangular block was 5" inches when measured from the top edge of the sheet. A drawing of the grid is shown in Fig. 8.

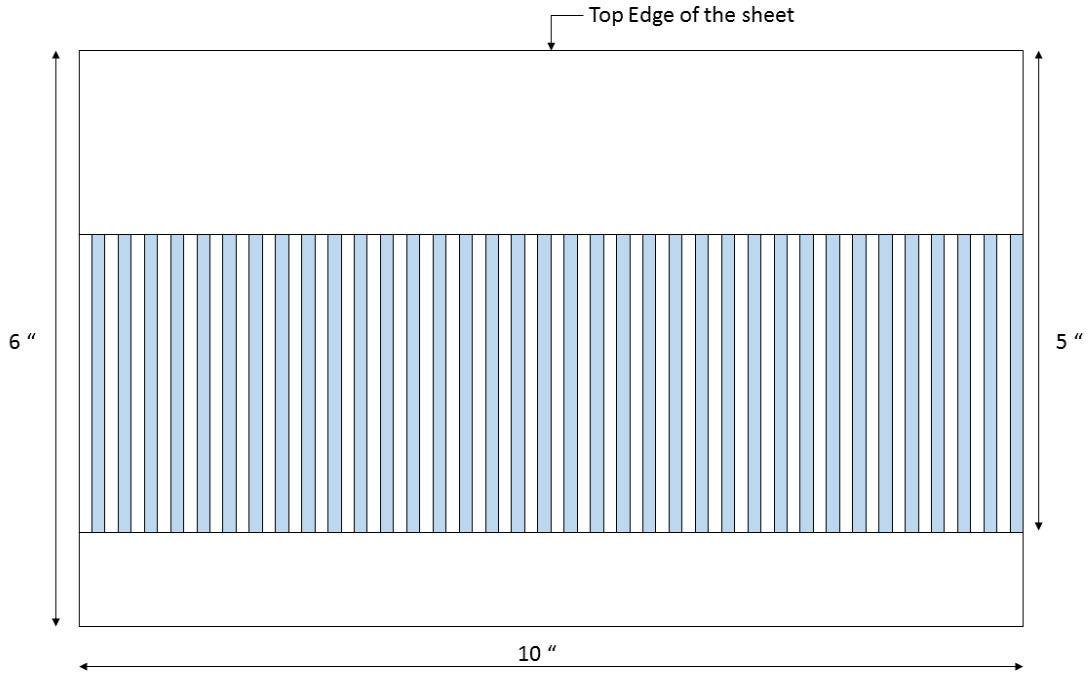

Figure 8: Angle Measurement Grid

Alternate rectangular blocks were cut out from the sheet and are represented by the blue rectangles in Fig.8. The sheet of paper was then wrapped around the cylinder such that the 10” side was along the circumference of the cylinder and the top edge of the sheet coincides with the edges of the cylinder. Each Vertex from the cut out cylinders lies at an angular increment of 5˚ from the previous vertex and coincide with the mid-span of the cylinder.

3.2.7 Jet Temperature Measurement

For an isothermal jet, only the ambient temperature was measured while for the cold jet in addition to the ambient, temperatures were measured at the jet centerline at the duct exit and just before impingement. These measurements were made using a T Type thermocouple connected to a NI 9213 thermocouple module mounted on a NI cDAQ 9172 USB chassis. Data was acquired using LabVIEW 2015 at a sampling frequency of 1 Hz. Each temperature measurement sequence was saved in a separate file for reference at a later stage.

3.3 Experimental Procedure

The experimental procedure for both the isothermal and the cold jets were very similar. The impinging distance between the fan the cylinder was adjusted to the desired value using a tape measure and the angle measurement grid was attached to the cylinder. The IR camera was used to view the front portion ($\theta=0^{\circ}$ to $\theta=90^{\circ}$) of the cylinder as shown in Fig. 9 and the grid vortices were marked on the IR image stream using FLIR tools. Successive markings on the IR image represented 5° increments in circumferential angle along the cylinder surface. The grid was detached from the cylinder and the fan was switched on and the experiment was run till the cylinder reached steady state. Steady state was assumed when the temperature variations in all the marked points did not exceed 0.2 $^{\circ}$C over a period of 5 minutes. 2 IR images of the cylinder in steady state were saved. The angle measurement grid was reattached to the cylinder and the IR camera was moved to view the rear side of the cylinder($\theta=95^{\circ}$ to $\theta=180^{\circ}$) and the corresponding locations were marked on the IR image stream .The grid was then removed from the cylinder and experiment was allowed to run till the points marked on the rear side reached steady state. The heater was switched off and the cylinder was removed from the supports so that the velocity and temperature measurements could be made on a free jet. Jet centerline velocity and in the case of cold jets, jet centerline temperatures were measured and recorded at the desired impinging distance. The cylinder was allowed to cool down to room temperature before the experiment was repeated at the next impinging distance.

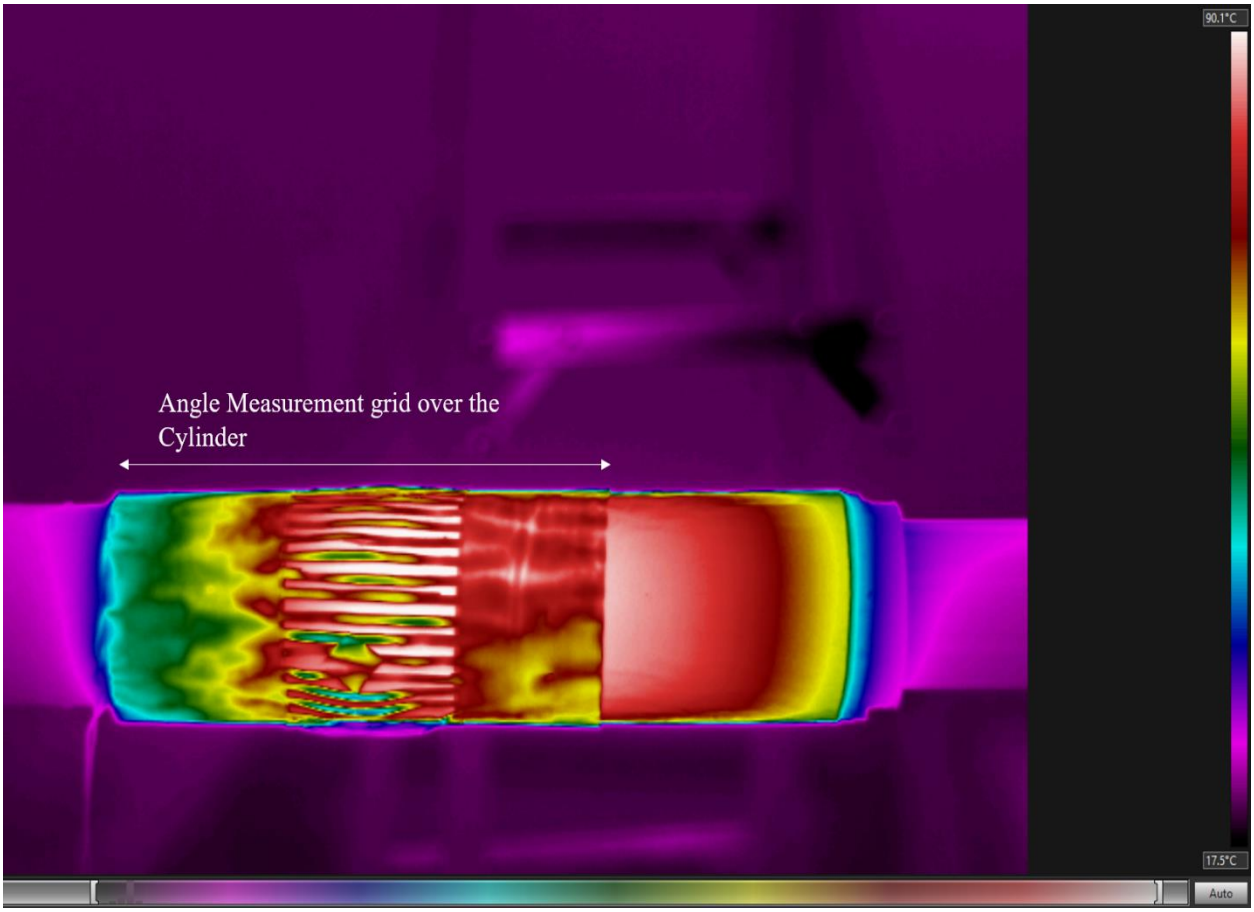

Figure 9: IR Image of the Grid Wrapped Around a Cylinder

3.4 Data Reduction

With the temperature distribution along the cylinder circumference, the distribution of local heat transfer coefficient at each impinging distance can be calculated. The total power supplied by the AC Variac to the heater is given by the equation

$$q_{total} = \frac{V^2}{R} \tag{9}$$

Where V is the RMS voltage measured by the Multimeter and is equal to 60V the isothermal jet and 61.5 V for the cold jet, R is the heater resistance and is measured to be 60 Ω for the Minco heater used in isothermal jets and 56 Ω for the screen printed heater used in vertical cold jets.

Thus the net heat flux supplied to the heater is

$$q"_{total} = \frac{q_{total}}{A_s} \tag{10}$$

Where A_s is the surface area of the heater and its value is 0.0645 m^2 for the isothermal jet heater and 0.0516 m^2 for the heater used in cold jets.

The total convective heat flux between the heated cylinder and the impinging jet is calculated as

$$q"_{conv} = q"_{total} - q"_{rad} - q"_{cond,z} - q"_{cond,r} \tag{11}$$

Where, $q"_{rad} = \varepsilon\sigma(T_{local}^4 - T_\infty^4)$ is the net loss in heat flux due to radiation

$q"_{cond,z}$ = conduction loss in through the back of the cylinder $= \dfrac{T_{local} - T_\infty}{\left(\dfrac{\ln(\frac{r_3}{r_2})}{2\pi k_{rubber}} + \dfrac{\ln(\frac{r_2}{r_1})}{2\pi k_{PVC}}\right)}$

$q"_{cond,r}$ = conduction correction in the circumferential direction $= -k_{al} t_{al} \dfrac{\partial^2 T}{\partial x^2}$

Where r_3 is the outer radius of the cylinder with the rubber, r_2 and r_1 are the outer and inner radius of the PVC pipe respectively, t_{al} is the thickness of the aluminum foil on the heater(0.005") and $k_{rubber}, k_{PVC}, k_{al}$are the thermal conductivities of the rubber, PVC pipe and aluminum foil respectively.

The value of $\frac{\partial^2 T}{\partial x^2}$ is obtained by curve fitting the local temperature distribution of the cylinder along the circumference of the cylinder and by calculating the second derivative of the regression equation.

The local heat transfer coefficient for an isothermal jet is determined by the equation

$$h_{local} = \frac{q"_{conv}}{T_{local} - T_\infty} \tag{12}$$

However, in case of the cold jet the local heat transfer coefficient can be calculated based on two temperatures of the impinging jet; temperature of jet centerline at origin of the jet (T_0) and the local temperature of the jet centerline at the stagnation point (T_j) and are given by the expressions

$$h_0 = \frac{q"_{conv}}{T_{local} - T_0} \tag{13}$$

$$h_j = \frac{q"_{conv}}{T_{local} - T_j} \tag{14}$$

The local Nusselt Number is calculated using the local heat transfer coefficient as

$$Nu = \frac{hD}{k} \tag{15}$$

Where, k is the thermal conductivity of air calculated at film temperature.

For a cylinder in crossflow with a uniform flow, the Frossling number is defined as the ratio of Nusselt number and the square root of the Reynolds number. The local Frossling number in case of an impingement jet is defined as

$$Fro = \frac{Nu}{\sqrt{Re_D}} \tag{16}$$

Where, Nu is the local Nusselt number and Re_D is the Reynolds number based on the cylinder diameter and is given by the expression

$$Re_D = \frac{\rho_0 U_0 D}{\mu} \tag{17}$$

Where, ρ_0 is the density of the air at the jet exit, U_0 is the jet exit velocity ,D is the cylinder Diameter and μ is the dynamic viscosity at the jet exit centerline temperature T_0. The density ρ_0 is calculated using the ideal gas law given as

$$\rho_0 = \frac{P_0}{R_a T_0} \tag{18}$$

The jet exit velocity U_0 is calculated from the formula

$$U_0 = \sqrt{\frac{2\Delta P}{\rho_0}} \tag{19}$$

Where, ΔP is the differential pressure reading of the manometer connected to the pitot tube.

The circumferential average Nusselt number is obtained by integrating the value of local Nusselt over the entire cylinder circumference (θ=0˚ to θ=360˚). However, since the Nusselt number distribution is assumed to be symmetric about the stagnation point along the circumference, the Average Nusselt number as defined by [26] is expressed as

$$Nu_{avg} = \int_{\theta=0^{\circ}}^{\theta=180^{\circ}} Nu \, d\theta \tag{20}$$

The average circumferential Frossling number is also calculated in a similar way.

Chapter 4: Results and Discussion

In this section the effect of impinging distance on the centerline velocities, centerline temperatures, local Frossling number distribution and the average Frossling number for the isothermal jets and the two cold jets are studied and compared against each other. A difference of 11% is noticed in the Reynolds number of the isothermal (Re_D=60000) and the non-isothermal jets(Re_D=67000) due to variations in jet velocities from the corresponding fans that are used to produce the jets. Hence the corresponding Frossling numbers of the isothermal and cold jets are used to compare heat transfer results. Table 1 summarizes the Uncertainties in the Frossling numbers as calculated in Appendix B

Frossling Number Type	Average Uncertainty	Highest Uncertainty	Lowest Uncertainty
Local Fro at $\theta \leq 80^{\circ}$	5.8%	6.7%	4.5%
Local Fro at $\theta \geq 80^{\circ}$	9.8%	10.6%	9.3%
Average Fro	5.8%	6.7%	4.5%

Table 1:Summary of Frossling number Uncertainty

4.1 Variation of Centerline Velocity with Distance

Figure 10 shows the variation of the normalized centerline velocity of the three free jets with distance. For all the three jets, the centerline velocity remains constant from the jet exit till a distance of Z/d=4. At Z/d=8, the centerline velocity of all the three jets begin to drop off due to the continuous entrainment of the ambient fluid. This shows that the potential core length for all the three jets is somewhere between Z/d=4 to Z/d=8. The study done by Wang et al. [10] showed many researchers reporting potential core lengths between Z/d=4 and Z/d=7.7 depending upon the type of nozzle used to produce the jet and the Reynolds number at jet exit. The velocity decay continues up to the last measured distance of Z/d= 20 as the entrainment effects of the ambient air continuously increases. Since the number of measurement points in the current experiment are limited, a correlation to quantify the velocity decay is expected to contain significant errors. The values of the normalized centerline velocity of the isothermal jets compare well with the results of

Malmström et al.[27]who measured the decay of centerline velocity of low velocity impinging jets.

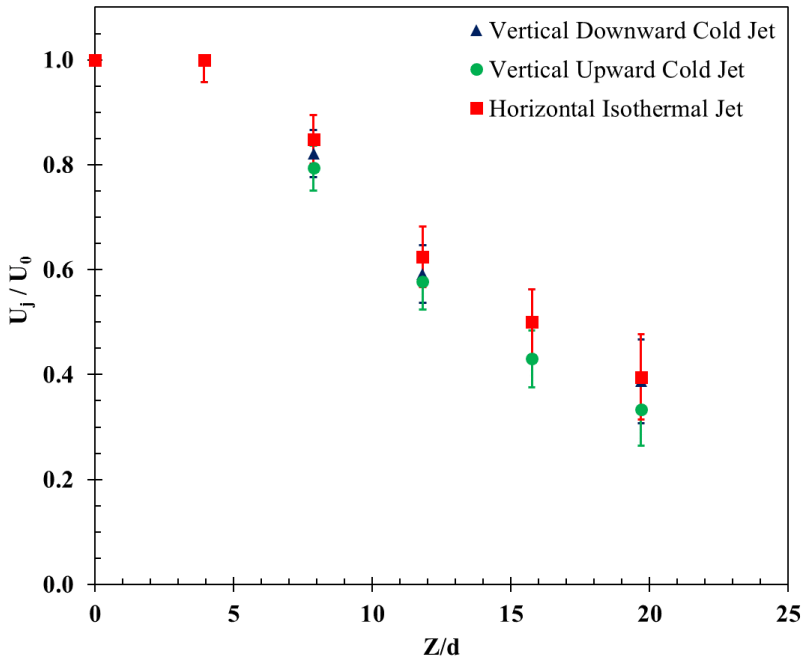

Figure 10: Variation of Centerline Velocity with Distance

At all impinging distances, the values of the normalized velocity of all the three jets are close to each other and any differences observed lie within the experimental uncertainty. The close proximity of the normalized velocity values of the cold jets to the isothermal jet show that the buoyancy effect is negligible when compared to the momentum effects in the range of distances used and the magnitude of temperature difference between the jet and the ambient at the jet exit (ΔT_0).Hollworth et al. [28] measured the centerline velocities at various axial locations of a heated jet (ΔT_0 of 30˚C and 60˚C) discharged vertically downwards and compared it against an isothermal jet .They concluded that the axial decay of centerline velocity for the heated jet is virtually similar to that of the isothermal jet due to low values of ΔT_0.

The centerline velocities of the two cold jets were scaled based on the jet exit Froude number for comparisons against correlations obtained by Ogino et al.[15]. Table 2 summarizes the values of the Froude numbers and ΔT_0. The variations in ΔT_0 are due to changes in temperature of the cold jet drawn from outdoors.

Figure 11 shows a comparison of the centerline velocity variation of the downward and upward cold jet with that the correlation obtained by Ogino et al.[15] for the Froude numbers used in Table

2. The X axis is scaled as $Z/(d*Fr^{0.5})$ and the Y axis is scaled as $Fr^{0.5}*(U_j/U_0)$. The centerline velocities for the downward cold jet is higher than the values obtained from the correlation with the highest difference of 24% at Z/d=20. The values of centerline velocities of the upward cold jet are slightly closer to the correlation with a highest difference of 15% occurring at Z/d=8.

Impinging Distance (Z/d)	**Downward Cold Jet**		**Upward Cold Jet**	
	ΔT_0	**Froude Number**	ΔT_0	**Froude Number**
4	12.05	3204	13.5	1930
8	11.6	3328	10.3	2530
12	12.3	3139	13.2	1974
16	12	3217	9	2895
20	12.3	3139	11.85	2199

Table 2:Summary of Froude numbers and Temperature gradients

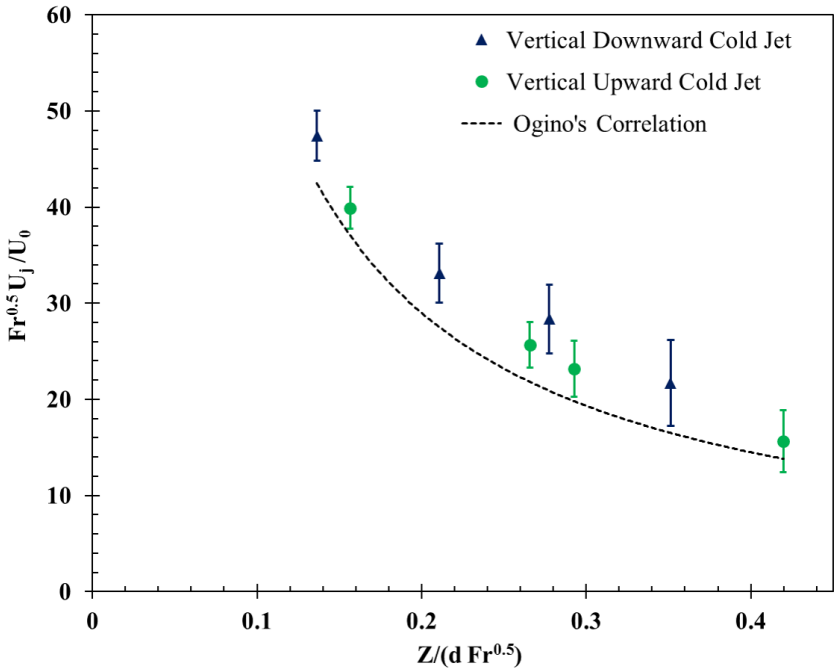

Figure 11: Comparison of Centerline Velocity of Cold Jets with Ogino's Correlation

4.2 Variation of Centerline Temperature with Distance

In the case of free cold jets, the difference between centerline temperature at a given distance and the ambient temperature (ΔT_j) is normalized with respect to the difference between centerline temperature at the jet exit and the ambient temperature (ΔT_0). Figure 12 shows the variation of the normalized jet centerline temperature with impinging distance for both discharge directions of the cold jet. Unlike velocity, the decay of centerline temperature starts at Z/d=4. Sfeir[29] reported that the temperature distribution potential core is shorter than the velocity potential core of the jet due to a faster spread of temperature .

The maximum temperature difference in the non-dimensional temperatures for the cold jets was 14% at distance of Z/d=16. When high relative uncertainties in low temperature measurement are taken into account, the close proximity of the values suggests that the jet centerline temperature is not affected by the direction of the jet.

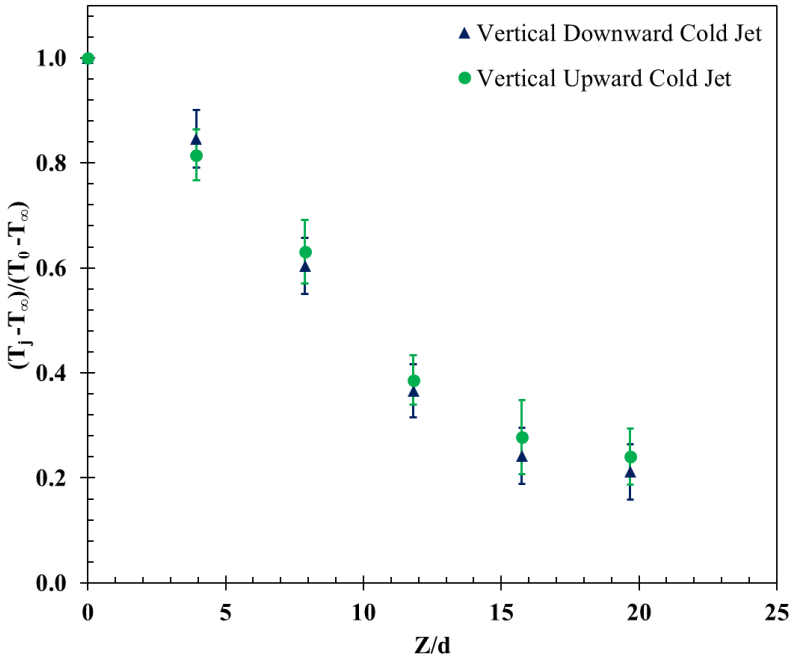

Figure 12: Variation of Centerline Temperature with Distance

Figure 13 shows the comparison of the temperature decay with the correlations obtained by Ogino in equation 6.

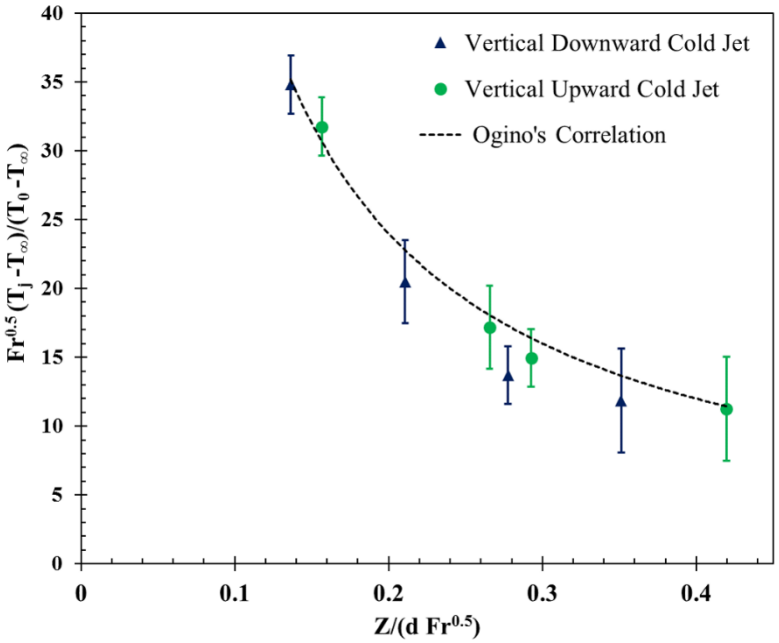

Figure 13: Comparison of Centerline Temperature of Cold Jets with Ogino's Correlation

The measured temperature values are very close to Ogino's correlations. The downward cold jet had a maximum difference of 20% from the correlations at Z/d =16 while the upward cold jet had a maximum deviation of 9% at Z/d =16.

4.3 Stagnation Frossling number

4.3.1 Based on Jet Impingement Temperature ($Fro_{stag,\ j}$)

Figure 14 shows the variation of stagnation Frossling number with distance for the isothermal jet and the two cold jets. In case of the cold jets, the stagnation Frossling is calculated based on the temperate difference between the cylinder and the centerline impinging temperature of the jet (T_j). For the isothermal jet, the stagnation Frossling number ($Fro_{stag,\ iso}$) increases from Z/d=4 to Z/d=8 by about 15% even though the centerline velocity decreases. A similar trend was observed by Lee et al. [13] in their experiments for a cylinder of curvature ratio D/d=10.6 over a wide range of Reynolds numbers. According to Gardon and Akfirat [12], the increase in stagnation point heat transfer till Z/d =8 is attributed to increase in centerline turbulence reaching its peak at Z/d =8. Their study shows that the turbulence level is nearly constant beyond a distance of Z/d =8-10.

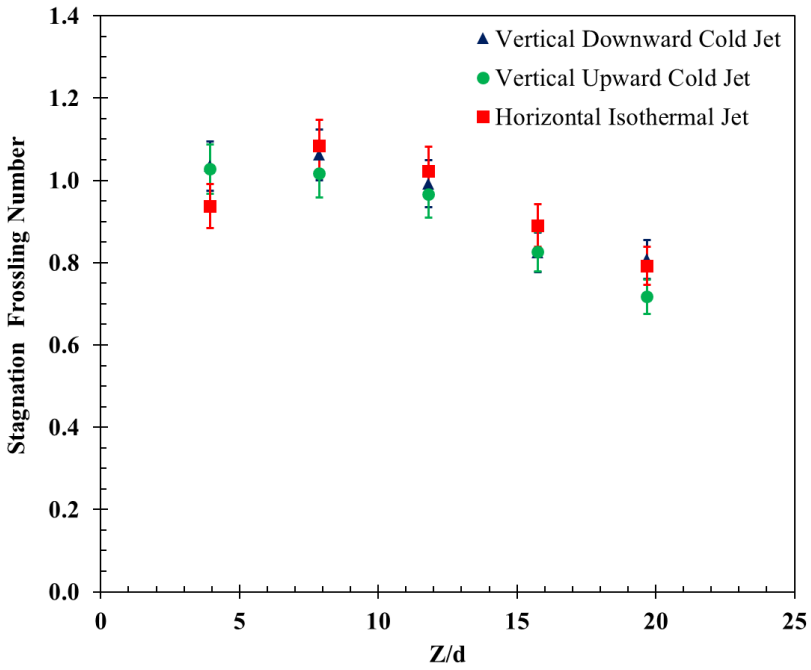

Figure 14: Variation of Jet Impinging Temperature based Stagnation Frossling Number with Distance

Beyond Z/d=8, $Fro_{stag,\ iso}$ decreases continuously till Z/d =20 as the decay of the centerline velocity starts dominating over the nearly constant turbulence level that occurs beyond Z/d=8. In case of both cold jets, the $Fro_{stag,\ j}$ nearly stays constant from the Z/d=4 to Z/d=8 beyond which, it starts decreases continuously till Z/d=20. The $Fro_{stag,\ j}$ for all the three jets lie close to each other at all impinging distances with a maximum difference of 10% occurring at Z/d=20.

4.3.2 Based on Jet exit temperature ($Fro_{stag,0}$)

Figure 15 shows the variation of stagnation Frossling number with distance for the isothermal jet and the two non-isothermal jets. In case of the cold jets, the stagnation Frossling number ($Fro_{stag,0}$) is calculated based on the temperate difference between the cylinder surface and the nozzle exit temperature of the jet (T_0).

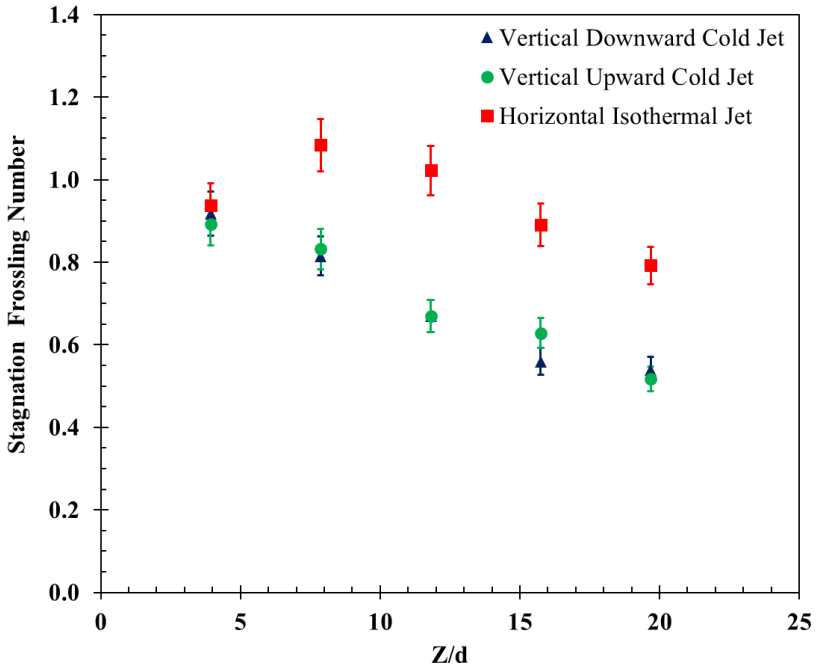

Figure 15: Variation of Jet Exit Temperature based Stagnation Frossling Number with Distance

Again, the Frossling number of the cold jets lie very close to each other. Except at Z/d=4, the $Fro_{stag,0}$ of the cold jets is much lower than the isothermal case because of the decrease in temperature of the jet with distance from the exit. There is a continuous decrease of $Fro_{stag,0}$ for both the cold jets from Z/d=4 to Z/d=20 and the rate of decrease for $Z/d \geq 8$ is much steeper than $Fro_{stag,\,j}$. This is attributed to the negative effects of thermal entrainment of the surrounding fluid which continuously decreases the centerline temperature of the colds jets. The difference between the $Fro_{stag,0}$ of the cold jets and the stagnation Frossling number of the isothermal is large at impinging distances $Z/d \geq 8$ with a maximum difference of 50 % occurring at Z/d=20.

4.4 Local Frossling Number Distribution along the cylinder circumference

Figure 16 shows the local distribution of the Frossling numbers of the isothermal (Fro_{iso}) and the two cold jets (Fro_j) at various impinging distances. The local Frossling number of the cold jets is calculated based on the centerline impinging temperature of the jet (T_j).

At Z/d =4, both the jets are in the potential core of the incoming jet and Fro_{iso} decreases continuously from the stagnation point till it reaches a local minimum at $\theta = 80^{\circ}$. This is the flow separation point after which Fro_{iso} increases monotonically till $\theta = 180^{\circ}$. The distribution of Fro_{iso} is similar to that of a cylinder immersed in cross flow on a uniform flow [10] and compares well

with the results of Sanitjai and Goldstein [30] who performed heat transfer measurements for a cylinder immersed in a crossflow over a wide range of Reynolds numbers(44000-89200). The trends of circumferential distribution of Fro_j for both the cold jets resemble each other. There is a decrease in Fro_j from stagnation point till $\theta = 80^\circ$. A secondary minima occurs at about $\theta = 140^\circ$ after which the Fro_j increases till $\theta = 180^\circ$.

At Z/d=8, differences can be noted in the Fro_{iso} and Fro_j distribution in the rear of the cylinder ($\theta \geq 80^\circ$) when compared to the corresponding trend at Z/d=4. In case of Fro_{iso} , secondary local maxima and minima occur at $\theta=105^\circ$ and $\theta=150^\circ$respectively .This can be attributed to the increasing turbulence of the impinging jet due to its interaction with the surrounding fluid. Once again, the Fro_j of both the cold jets are identical and very close to each other. The secondary maxima and minima disappear and the Frossling number decreases continuously till about at $\theta=150^\circ$ beyond which it remains constant.

At Z/d=12, the Fro_{iso} from $\theta=90^\circ$ to $\theta=105^\circ$ is nearly constant and then decrease till $\theta=150^\circ$. The Fro_j has nearly the same distribution as that at Z/d=8. The circumferential distributions of Fro_{iso} and Fro_j at Z/d=12 and Z/d=16 are both similar to their corresponding distributions at Z/d=12. This can be attributed to fully developed velocity and temperature profiles of the impinging jet at $Z/d \geq 12$.

Figure 22 in Appendix A show the circumferential distribution of Fro_0 and Fro_{iso} at various impinging distances. At impinging distances Z/d>4, the values of Fro_0 at all angles around the cylinder circumference is lesser than the corresponding values of Fro_j. This is because the jet temperature is continuously decreasing from its origin. Similar results were obtained by Hollworth[31] who compared the heat transfer results for a flat plate being impinged by isothermal and non-isothermal hot jets.

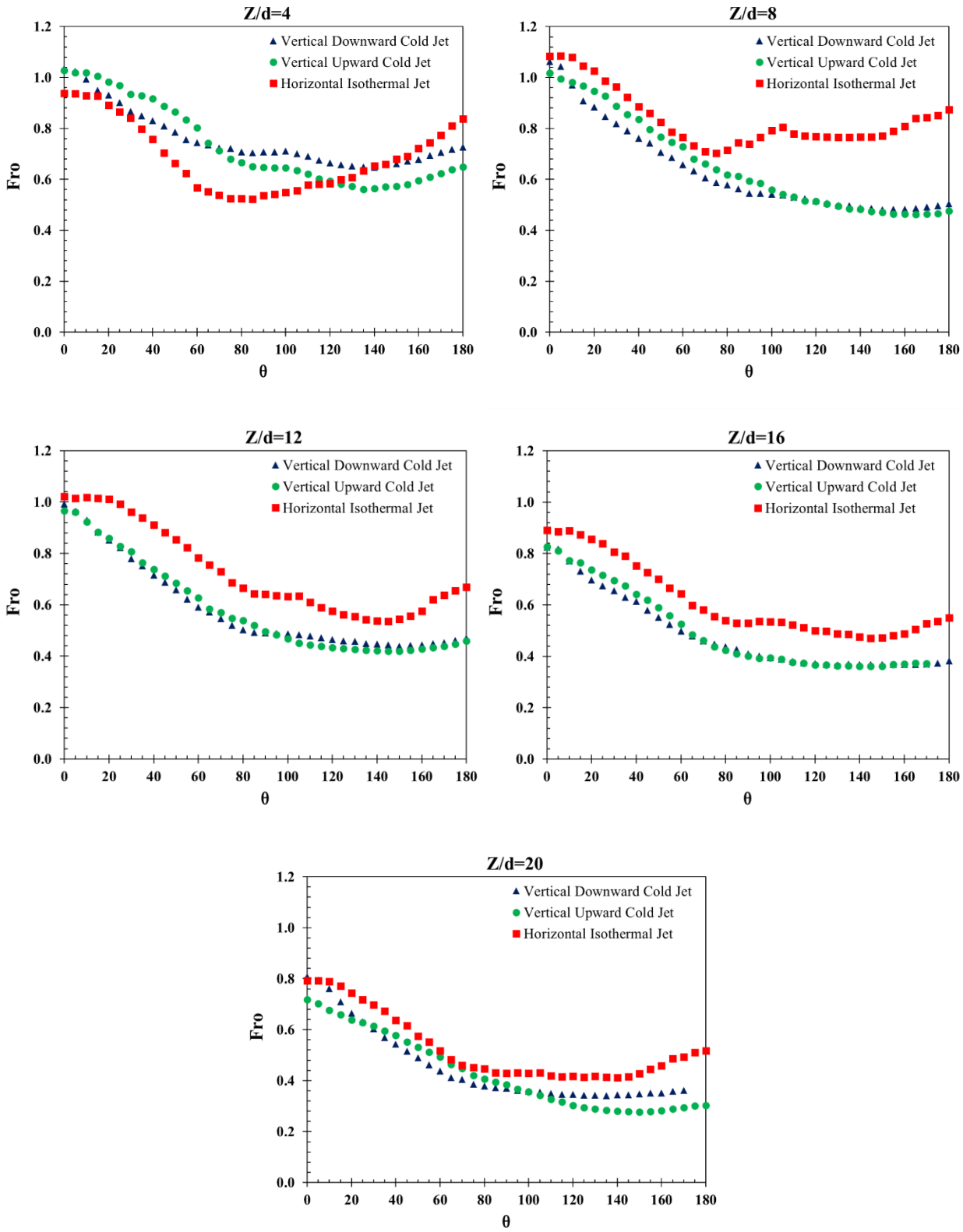

Figure 16: Local Distribution of Isothermal and Jet Impinging Temperature based Frossling Numbers from Z/d=4 to Z/d=20

4.5 Local Frossling number distribution along the cylinder axis

In addition to the circumferential direction, the local Frossling number distribution was also investigated in the axial direction along the stagnation point. Figure 17 shows the IR image of the temperature distribution in the stagnation region of the cylinder impinged by the upward cold jet at a distance of Z/d=4. The image shows that the temperature along both the cylinder axis and the circumferential direction is symmetric about the stagnation point.

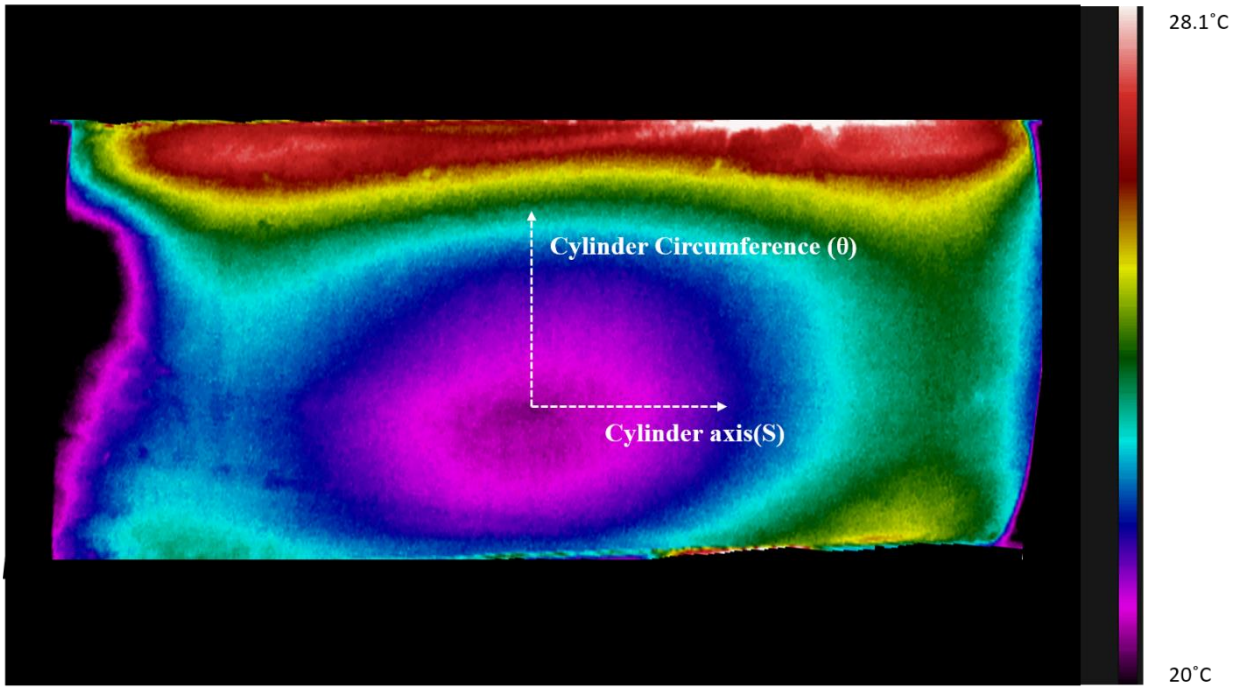

Figure 17: IR Image of the Front Portion of a Cylinder at Z/D=4 for an Upward Cold Jet

Figures 18 and 19 show the variation of local Frossling numbers along the cylinder axis when it is impinged by the horizontal isothermal and upward cold jet respectively. The distance along the cylinder axis is normalized with respect to the jet diameter at its origin and denoted by S/d. In case of the isothermal jet, the Frossling number distribution is very uniform about the stagnation point at all impinging distances. The plots show the trends only at Z/d=4 and Z/d=20 as most of the data at the other impinging distances overlap with the depicted plots. The highest variation is noticed at a distance of Z/d=4, where the stagnation point (S/d=0) Frossling number is about 5% higher than the corresponding value at S/d= $\pm$0.6. At greater impinging distances, the variation in Frossling numbers along the cylinder axis is further reduced and differences smaller than 2% are observed at Z/d=20.

The Frossling number distribution of the downward cold jet is identical to that of the upward cold jet and hence is not shown in the plots. At Z/d=4, the variation in Frossling number along the cylinder axis is more pronounced than the isothermal jet and the highest difference observed is 13% between S/d= $\pm$ 0.6 and S/d=0. This difference is reduced to 6% at Z/d=12 and is lowest at Z/d=20 where it is less than 3%.

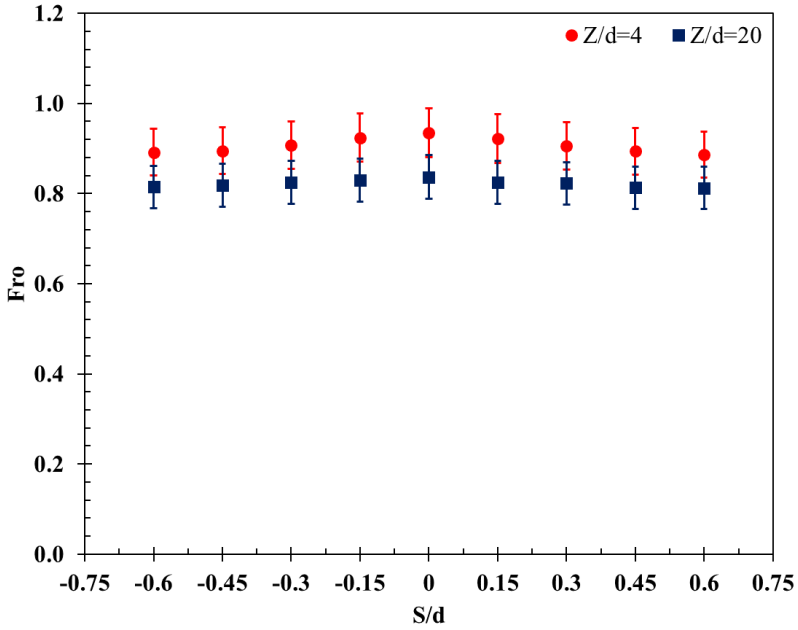

Figure 18: Frossling Number distribution along the Cylinder axis for the Horizontal Isothermal Jet

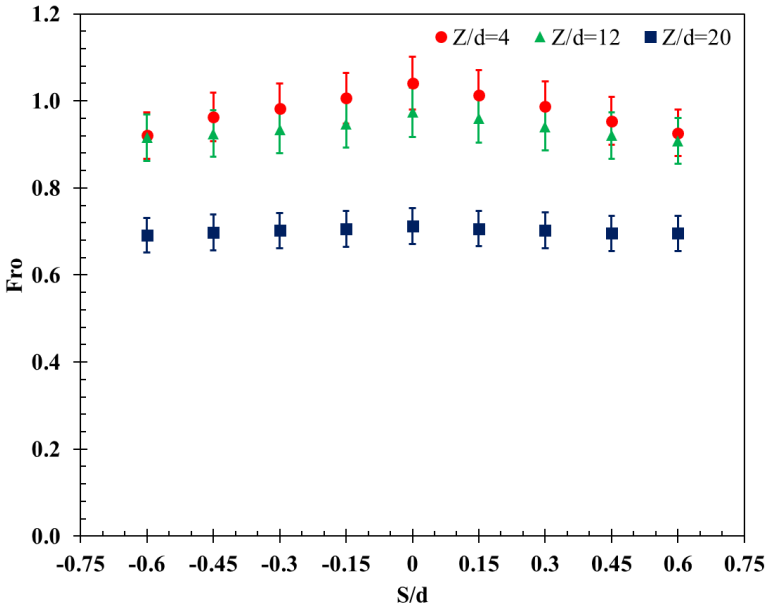

Figure 19: Frossling Number distribution along the Cylinder axis for the Upward Cold Jet

4.6 Average Frossling Number

The peripheral or the circumferential average Frossling number is calculated by integrating the Frossling numbers over the entire circumference of the cylinder similar to equation 20. In this experiment the average values for the isothermal and the non-isothermal jets are obtained numerically for each impinging distance and compared to each other.

4.6.1 Based on Jet Impingement Temperature ($Fro_{avg,\ j}$)

Figure 20 shows the variation of Average Frossling numbers of the isothermal and the cold jets with respect to impinging distance. The trends in the variation of the average Frossling numbers of the Isothermal Jets ($Fro_{avg,\ iso}$) and the cold Jets ($Fro_{avg,\ j}$) is similar to the trends in the variation of their respective Stagnation Frossling numbers. $Fro_{avg,\ iso}$ increases by about 21% from Z/d =4 to Z/d=8. It then reduces at a uniform rate of 14% at each impinging distance from Z/d =12 to Z/d=20.The overall reduction in the average Frossling number from Z/d=4 to Z/d=20 is 25%. The $Fro_{avg,\ j}$ for both the cold jets have nearly the same values at all impinging distances and monotonically decrease from Z/d=4 to Z/d=20 with an overall rate of 40%.

At Z/d=4 the $Fro_{avg,\ iso}$ and $Fro_{avg,\ j}$ is close with a difference of less than 10%. However, at all other impinging distances, $Fro_{avg,\ iso}$ is higher than $Fro_{avg,\ j}$ of the cold jets with the maximum difference of 33% occurring at Z/d=8. A potential cause for this is the non-uniformity of the temperature profile of the impinging jet at any cross-section due to the thermal entrainment effects of the surrounding fluid. Since the Frossling numbers for the cold jets are calculated solely based on centerline temperature of the impinging jet, the temperature profile of the imping jet is not taken into account.

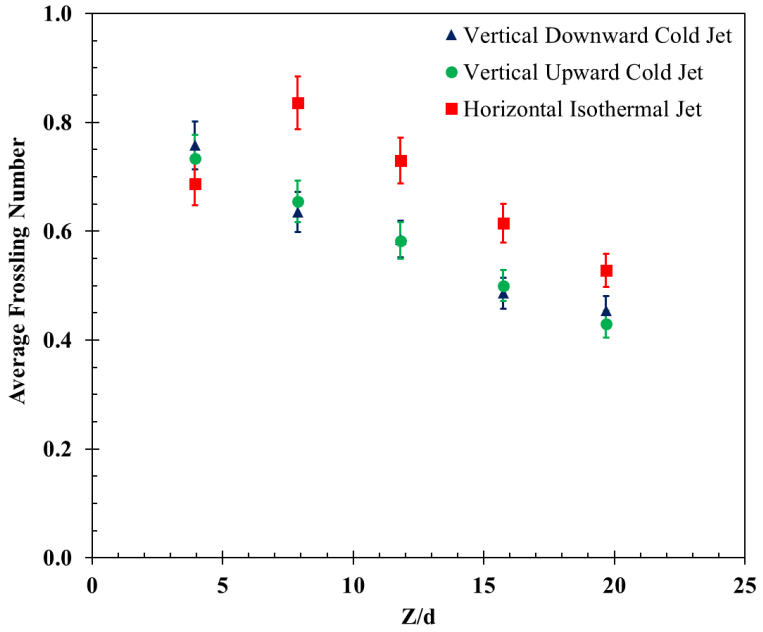

Figure 20: Variation of Jet Impinging Temperature based Average Frossling Number with Distance

4.6.2 Based on Jet exit temperature ($Fro_{avg,0}$)

The $Fro_{avg,0}$ for both the vertical cold jets are close to each other with a maximum difference of 10% occurring at Z/d=16. At Z/d=4 the $Fro_{avg,\ iso}$ and $Fro_{avg,\ j}$ of both the jets are close with a difference of less than 5%. At subsequent distances, $Fro_{avg,0}$ is always lower than the corresponding $Fro_{avg,\ j}$.

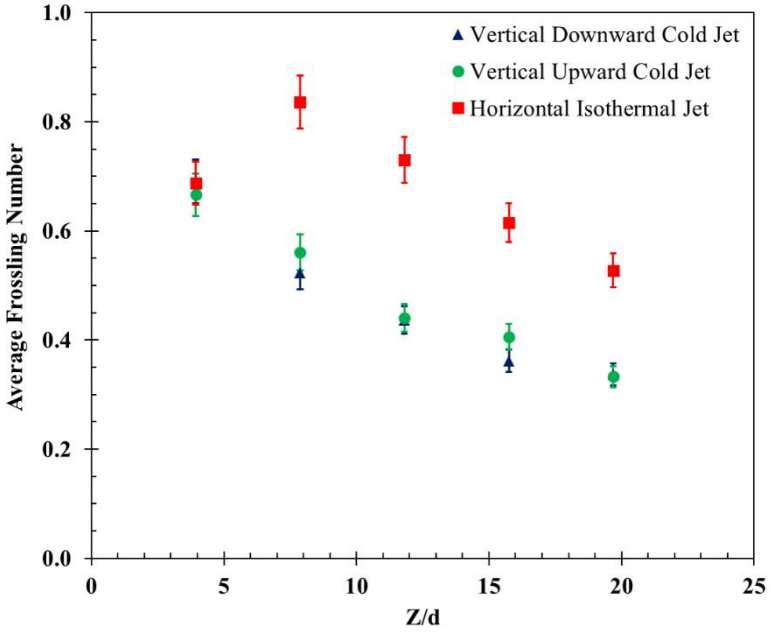

Figure 21: Variation of Jet Exit Temperature based Average Frossling Number with Distance

Chapter 5: Conclusions and Scope for Future Work

5.1 Conclusions

Heat transfer measurements were made on a heated cylinder impinged by a horizontal isothermal, vertically upward and vertically downward cold jets at selected distances from the jet origin. The results show that the distribution of Frossling number around the cylinder circumference at a given impinging distance is primarily dependent on the velocity, temperature and the turbulence characteristics of the incoming jet. Both the vertically upwards and downward discharged cold jets yield identical heat transfer rates at all impinging distances indicating that the buoyancy effects are negligible in the range of impinging distances and jet temperatures used in the experiments. Comparisons between the isothermal and the cold jets show that the stagnation Frossling numbers, $Fro_{stag,\ iso}$ and $Fro_{stag,\ j}$ are close to each other at all impinging distances. The circumferential distribution of Fro_{iso} and Fro_{j} at Z/d=12 is found to be similar to the corresponding distributions at Z/d=16 and 20. However, differences can be observed in the heat transfer rates of the cold and the isothermal jets especially at larger distances from the jet exit. From Z/d=4 to Z/d=20, the overall decrease in average Frossling number for the isothermal jet was found to be 25% with a peak value at Z/d =8 while the overall decrease of average Frossling number for both the cold jets was found to 40% with the peak occurring at Z/d=4. Even though the normalized centerline velocity characteristics of the isothermal and cold jets are found to be similar at all impinging distances, the non-uniform cross-sectional temperature profile of the cold impinging jets is identified as a potential cause for the difference in the average Frossling numbers.

Overall, it can be concluded that the isothermal and the non-isothermal jets provide substantial heat transfer rates at large impinging distances even though the velocities at such distances are significantly lesser than at the jet exit. This shows that the impinging jets can be considered an effective means of creating thermally conditioned microenvironments in a given building space

5.2 Scope for Future Work

In the current study, only the heat transfer from a human arm mimicked by a heated cylinder in a microenvironment created by the impinging jets is studied. A study of heat transfer rates from other organs like the head and legs using a heated mannequin would provide for a more detailed understanding of the overall response of the human body located in the microenvironment. Also

since the impinging jets used in the experiments are normal to the target surface, heat transfer results for an oblique jet impinging on human organs would aid in determining the most efficient orientation of the jet. Also a detailed comparison between the impinging jets and some of the commercially available microenvironment units would also aid in understanding the benefits and drawbacks of using these systems in a commercial building.

References

[1] Hamilton, S. D., Roth, K. W., and Brodrick, J., 2003, "Using microenvironments to provide individual comfort," ASHRAE J., **45**(9), pp. 65–66.

[2] Tsuzuki, K., Arens, E., Bauman, F., and Wyon, D., 1999, "Individual thermal comfort control with desk-mounted and floor-mounted task/ambient conditioning (TAC) systems," Proceedings of Indoor Air '99,Volume 2, pp. 368–373.

[3] Abramovich, G. ., and Schindel, L., 2003, The Theory of Turbulent Jets, MIT Press.

[4] Ashforth-Frost, S., and Jambunathan, K., 1996, "Effect of nozzle geometry and semi-confinement on the potential core of a turbulent axisymmetric free jet," Int. Commun. Heat Mass Transf., **23**(2), pp. 155–162.

[5] Martin, H., 1977, "Heat and Mass Transfer between Impinging Gas Jets and Solid Surfaces," Adv. Heat Transf., **13**(C), pp. 1–60.

[6] Coussirat, M., van Beeck, J., Mestres, M., Egusguiza, E., Buchlin, J.-M., and Escaler, X., 2005, "Computational Fluid Dynamics Modeling of Impinging Gas-Jet Systems: I. Assessment of Eddy Viscosity Models," J. Fluids Eng., **127**(4), p. 691.

[7] Jambunathan, K., Lai, E., Moss, M. A., and Button, B. L., 1992, "A review of heat-transfer data for single circular jet impingement," Int. J. Heat Fluid Flow, **13**(2), pp. 106–115.

[8] Giralt, F., Chia, C.-J., and Trass, O., 1977, "Characterization of the Impingement Region in an Axisymmetric Turbulent Jet," **16**(1), pp. 21–28.

[9] Cornaro, C., Fleischer, A. S., Rounds, M., and Goldstein, R. J., 2001, "Jet impingement cooling of a convex semi-cylindrical surface," Int. J. Therm. Sci., **40**(10), pp. 890–898.

[10] Wang, X. L., Motala, D., Lu, T. J., Song, S. J., and Kim, T., 2014, "Heat transfer of a circular impinging jet on a circular cylinder in crossflow," Int. J. Therm. Sci., **78**, pp. 1–8.

[11] Gori, F., and Bossi, L., 2000, "On the Cooling Effect of an Air Jet Along The Surface of a Cylinder," Intl.Comm.Heat Mass Transf., **27**(5), pp. 667–676.

[12] Gardon, R., and Akfirat, J. C., 1965, "The Role of Turbulence in Determining the Heat-Transfer Characteristics of Impinging Jets," Intl.J.Heat Mass Transf., **8**, pp. 1261–1272.

[13] Lee, D. H., Chung, Y. S., and Kim, D. S., 1997, "Turbulent flow and heat transfer measurements on a curved surface with a fully developed round impinging jet," Int. J. Heat Fluid Flow, **18**(1), pp. 160–169.

[14] Chen, C. J., and Rodi, W., 1980, Vertical turbulent buoyant jets: a review of experimental

data, Pergamon Press.

[15] Ogino, F., Takeuchi, H., Kudo, I., and Mizushina, T., 1980, "Heated Jet Discharged Vertically Into Ambients of Uniform and Linear Temperature Profiles.," Int. J. Heat Mass Transf., **23**(11), pp. 1581–1588.

[16] Mizushina, T., Ogino, F., Takeuchi, H., and Ikawa, H., "An experimental study of vertical turbulent jet with negative buoyancy," Wärme - und Stoffübertragung, **16**(1), pp. 15–21.

[17] Gillespie, M. B., Black, W. Z., Rinehart, C., and Glezer, a., 2006, "Local Convective Heat Transfer From a Constant Heat Flux Flat Plate Cooled by Synthetic Air Jets," J. Heat Transfer, **128**(10), p. 990.

[18] Donaldson, C. D., Snedeker, R. S., and Margolis, D. P., 1971, "A study of free jet impingement. Part 2. Free jet turbulent structure and impingement heat transfer," J. Fluid Mech., **45**(3), pp. 477–512.

[19] Sparrow, E. M., Altemani, C. A. C., Chaboki, A., and Experiments, T., 1984, "Jet-Impingement Heat Transfer for a Circular Jet Impinging in Crossflow on a Cylinder," J. Heat Transfer, **106**(August).

[20] Srinath, V. E., and Je-Chin, H., 2000, "A transient liquid crystal thermography technique for gas turbine heat transfer measurements," Meas. Sci. Technol., **11**(7), p. 957.

[21] Schroder, A., Ou, S., and Ghia, U., 2012, "Experimental Study of an Impingement Cooling-Jet Array Using an Infrared Thermography Technique," J. Thermophys. Heat Transf., **26**(4), pp. 590–597.

[22] Cherry, R. J., 2015, "Development of a Novel,Manufacturing Method of Producing Cost-Effective Thin-Film Heat Flux Sensors," Virginia Polytechnic Institute and State University.

[23] Carlomagno, G. M., and Cardone, G., 2010, "Infrared thermography for convective heat transfer measurements," Exp. Fluids, **49**(6), pp. 1187–1218.

[24] Cheng, T.-Y., Deng, D., and Herman, C., 2012, "Curvature Effect Quantification for in-Vivo Ir Thermography.," Int. Mech. Eng. Congr. Expo., **2**, pp. 127–133.

[25] Colban, W., Gratton, A., Thole, K. A., and Haendler, M., 2006, "Heat Transfer and Film-Cooling Measurements on a Stator Vane With Fan-Shaped Cooling Holes," J. Turbomach., **128**(1), p. 53.

[26] Tawfek, A. A., 1999, “Heat transfer due to a round jet impinging normal to a circular cylinder,” Heat Mass Transf., **35**(4), pp. 327–333.

[27] Malmström, T. G., Kirkpatrick, A. T., Christensen, B., and Knappmiller, K. D., 1997, “Centreline velocity decay measurements in low-velocity axisymmetric jets,” J. Fluid Mech., **246**, pp. 363–377.

[28] Hollworth, B. R., and Wilson, S. I., 1984, “Entrapment effects on impingement heat transfer: Part I — Measurements of heated jet velocity and temperature distributions and recovery temperatures on target surface,” J. Heat Transfer, **106**(November), pp. 797–803.

[29] Sfeir, A. A., 1976, “The velocity and temperature fields of rectangular jets,” Int. J. Heat Mass Transf., **19**(11), pp. 1289–1297.

[30] Sanitjai, S., and Goldstein, R. J., 2004, “Forced convection heat transfer from a circular cylinder in crossflow to air and liquids,” Int. J. Heat Mass Transf., **47**(22), pp. 4795–4805.

[31] Hollworth, B. R., and Gero, L. R., 1985, “Entrainment Effects on Impingement Heat Transfer: Part II—Local Heat Transfer Measurements,” J. Heat Transfer, **107**(4), p. 910.

[32] Moffat, R. J., 1988, “Describing the uncertainties in experimental results,” Exp. Therm. Fluid Sci., **1**(1), pp. 3–17.

Appendix A –Local Distribution of Frossling Number based on Jet exit temperature

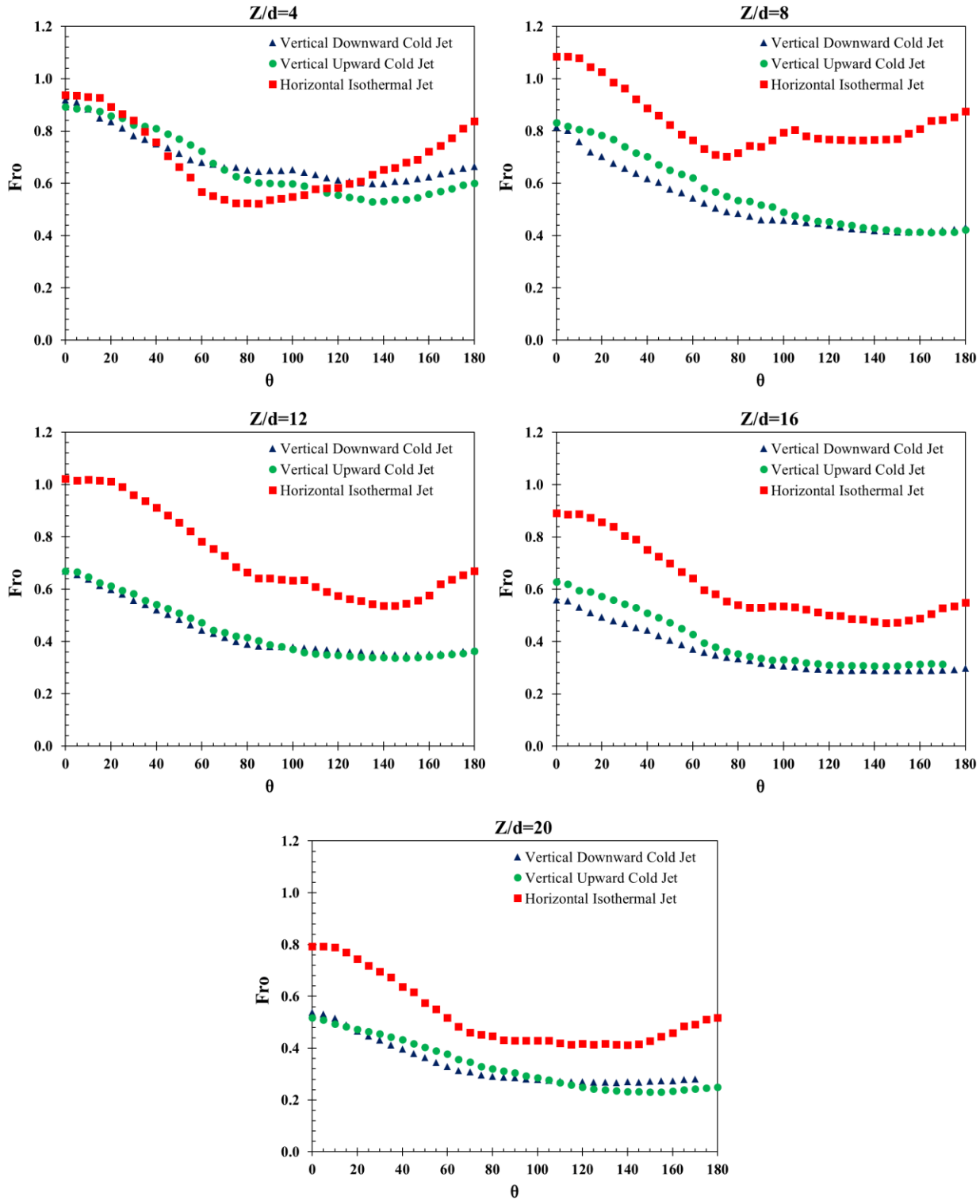

Figure 22: Local Distribution of Isothermal And Jet Exit Temperature based Frossling Numbers from Z/d=4 to Z/d=20

Appendix B: Uncertainty calculations

This section is used to estimate the uncertainties amongst various heat transfer parameters that affect the measurements performed in this thesis. The method suggested by Moffat[32] is used to determine the uncertainty values for Velocity, Frossling number and the Convective heat transfer coefficients.

B.1 Relative Uncertainty in Local Heat transfer coefficient in front portion of the cylinder (θ≤80˚)

The equation used in determining the total Convected heat flux from the cylinder to the jets in the results presented in the experiment is given by

$$q"_{conv} = q"_{total} - q"_{rad} - q"_{cond,z} - q"_{cond,r}$$

Substituting all the expressions from equation 11 gives

$$q"_{conv} = \frac{V^2}{A_s R} - \varepsilon\sigma(T_{local}^4 - T_\infty^4) - \frac{T_{local} - T_\infty}{\left(\frac{\ln\left(\frac{r_3}{r_2}\right)}{2\pi k_{rubber}} + \frac{\ln\left(\frac{r_2}{r_1}\right)}{2\pi k_{PVC}}\right)} - q"_{cond,r}$$

Where $q"_{cond,r} = -k_{al} t_{al} \frac{\partial^2 T}{\partial x^2}$ is the correction applied to account for the circumferential conduction across the cylinder. The variation of temperature is plotted with respect to x (the circumferential distance between the measurement points) and a sixth order polynomial regression equation is obtained. The second derivative of the regression equation ($\frac{\partial^2 T}{\partial x^2}$) is obtained and is used to calculate the conduction correction. It is seen that at all impinging distances, the curve fit is accurate from θ=0˚ to θ=80˚.Hence the correction is applied in the calculations of local Frossling number at these points. However, the curve fitted equation does not accurately depict the local maxima and local minima that occur at the rear of the cylinder(θ≥80˚). Hence the conduction correction is not included in the heat transfer calculations at the rear of the cylinder and hence considered in the uncertainty calculations performed in section B.2

For the front region of the cylinder, the sensitivity coefficients are

$$c_1 = \frac{\partial h}{\partial V} = \frac{2V}{RA_s}$$

$$c_2 = \frac{\partial h}{\partial T_{local}} = \frac{-V^2}{RA_s(T_{local} - T_\infty)^2} - \varepsilon\sigma(3{T_{local}}^2 + 2T_{local}T_\infty + {T_\infty}^2) - \frac{{q"}_{cond,r}}{(T_{local} - T_\infty)^2}$$

$$c_3 = \frac{\partial h}{\partial T_\infty} = \frac{V^2}{RA_s(T_{local} - T_\infty)^2} - \varepsilon\sigma(3{T_\infty}^2 + 2T_\infty T_{local} + {T_{local}}^2) + \frac{{q"}_{cond,r}}{(T_{local} - T_\infty)^2}$$

The uncertainty is the local heat transfer coefficient is given by

$$u_h = \sqrt{c_1^2\delta_1^2 + c_2^2\delta_2^2 + c_3^2\delta_3^2}$$

The relative uncertainty in local h is given by $\frac{u_h}{h}(\%)$

Parameter	Value of Uncertainty
Voltage	0.01 V
T_{local}	0.5˚C
T_∞	0.5˚C

Table 3:Uncertainty budget for local heat transfer coefficient for θ≤80˚

The relative uncertainty values of the local heat transfer coefficient till θ≤80˚ were averaged at all impinging distances and was found out to be 5.5%

B.2 Relative Uncertainty in Local Heat transfer coefficient in the rear portion of the cylinder (θ≥80˚)

The local convective heat transfer coefficient is given by

$${q"}_{conv} = \frac{V^2}{A_s R} - \varepsilon\sigma(T_{local}^4 - T_\infty^4) - \frac{T_{local} - T_\infty}{\left(\frac{\ln\left(\frac{r_3}{r_2}\right)}{2\pi k_{rubber}} + \frac{\ln\left(\frac{r_2}{r_1}\right)}{2\pi k_{PVC}}\right)} + {q"}_{cond,r}$$

$$h = \frac{{q"}_{conv}}{(T_{local} - T_\infty)}$$

The sensitivity coefficients are

$$c_1 = \frac{\partial h}{\partial V} = \frac{2V}{RA_s}$$

$$c_2 = \frac{\partial h}{\partial T_{local}} = \frac{-V^2}{RA_s(T_{local} - T_\infty)^2} - \varepsilon\sigma(3{T_{local}}^2 + 2T_{local}T_\infty + {T_\infty}^2) - \frac{({q"}_{cond,r})}{(T_{local} - T_\infty)^2}$$

$$c_3 = \frac{\partial h}{\partial T_\infty} = \frac{V^2}{RA_s(T_{local} - T_\infty)^2} - \varepsilon\sigma(3{T_\infty}^2 + 2T_\infty T_{local} + {T_{local}}^2) + \frac{({q"}_{cond,r})}{(T_{local} - T_\infty)^2}$$

$$c_4 = \frac{\partial h}{\partial {q"}_{cond,r}} = \frac{1}{(T_{local} - T_\infty)}$$

The uncertainty is the local heat transfer coefficient is given by

$$u_h = \sqrt{c_1^2\delta_1^2 + c_2^2\delta_2^2 + c_3^2\delta_3^2 + c_4^2\delta_4^2}$$

Where δ is the uncertainty associated with each parameter

Parameter	Value of Uncertainty
Voltage	0.01 V
T_{local}	0.5˚C
T_∞	0.5˚C
${q"}_{cond,r}$	8.6% of q" total

Table 4:Uncertainty Budget for Local heat transfer Coefficient for θ≥80˚

The uncertainty values of the local heat transfer coefficient till θ≤80˚ were averaged at all impinging distances and its value was found out to be 9.7% . Since the Nusselt number is a linear function of local heat transfer coefficient, the same value of uncertainty is applicable for local Nusselt number also.

B.3 Relative Uncertainty of Average Heat Transfer Coefficient

While determining the average heat transfer coefficient, the conduction along the circumference is neglected as the net conduction along the circumference is zero. Hence the relative uncertainty calculation must resemble that in the front portion of the cylinder. Hence the overall uncertainty in the average Frossling number is 5.5%.

B.4 Relative Uncertainty in Reynolds number

The jet centerline velocity is calculated based on the readings obtained by a pitot tube connected to a differential manometer. The accuracy of the manometer as specified by the manufacturer is

3% of the Full measurement scale of the manometer ($\delta_6 = 7.5$ Pa) .The velocity is calculated by the formula

$$U_0 = \sqrt{\frac{2\Delta P}{\rho_0}}$$

$$u(U_0) = \delta_6/(\sqrt{2\rho_0}\Delta P)$$

The relative uncertainties of the centerline exit velocities for all the three jets are found out to be 3.8%. Since the Reynolds number depends linearly on velocity, it is also found to have the same uncertainty of 3.8%.

B.5 Relative Uncertainty in Frossling number

The local Frossling number is calculated by the formula

$$Fro = \frac{Nu}{\sqrt{Re_D}}$$

The sensitivity coefficients are

$$c_7 = \frac{\partial Fro}{\partial Nu} = \frac{1}{\sqrt{Re_D}}$$

$$c_8 = \frac{\partial Fro}{\partial Re_D} = -\frac{Nu}{2}\frac{1}{{Re_D}^{3/2}}$$

The uncertainty in Local Frossling number is given by

$$u(Fro_{local}) = \sqrt{c_7^2\delta_7^2 + c_8^2\delta_8^2}$$

Parameter	Value of Uncertainty	Comments
Nusselt number	5.5% of Nu	Section B.1
Reynolds number	3.8% of Re_D	Section B.4

Table 5: Uncertainty budget for Local Frossling number(θ≤80˚)

The relative uncertainty for the local Frossling number at the front of the cylinder is found to be 5.8%. The relative uncertainty for the local Frossling number at the rear of the cylinder is found to be 9.8%. The uncertainty of the Average Frossling number resembles that of the of the front portion of the cylinder and is 5.8%.

Appendix C: Quantification of IR camera viewing angle

The viewing angle of the IR camera with respect to the cylinder surface has a significant effect on the temperature measurements. Previous studies show that viewing angles greater than 60˚ cause apparent temperature differences of more than 0.4 ˚C on a vertical cylinder with a uniform temperature boundary condition. This has been explained due to the variation of emissivity at high angles between the normal to the viewing surface and the direction of IR emission. Such differences can affect low temperature measurements causing high experimental uncertainties. Hence quantification of the viewing angle is required to be quantified to avoid the curvature effects of the cylinder.

The experimental set up consists of a vertical cylinder heated by a AC source producing uniform heat flux under natural convection. The cylinder is placed vertically so that the effect of natural convection is the same for along point along the circumference of the cylinder. The heater is powered by a DC power source and a voltage of 36 V is applied across the lead wires. The cylinder is viewed by an IR camera which is placed horizontally on Tripod. The angle measurement grid is placed on the cylinder surface and the 5˚ angles are marked on the cylinder surface. The grid is detached from the surface and the cylinder is allowed to reach a steady value. The variations in the marked points are recorded and the viewing angle is determined as the angular displacement between points on both sides of the normal to cylinder surface which have a maximum temperature difference of 0.2˚C.

Figure 23 shows the vertical cylinder viewed by the IR camera. The edges of the cylinder appear to be colder than the core region of the jet due to the viewing angles. The ends of dotted line on the image show the threshold points beyond which the temperature of the jet starts to drop off significantly. The ends of the line are at angle 110˚ from each other and hence the viewing angle for the IR camera used in the current experiment is quantified as $\pm$ 55 ˚ from the normal.

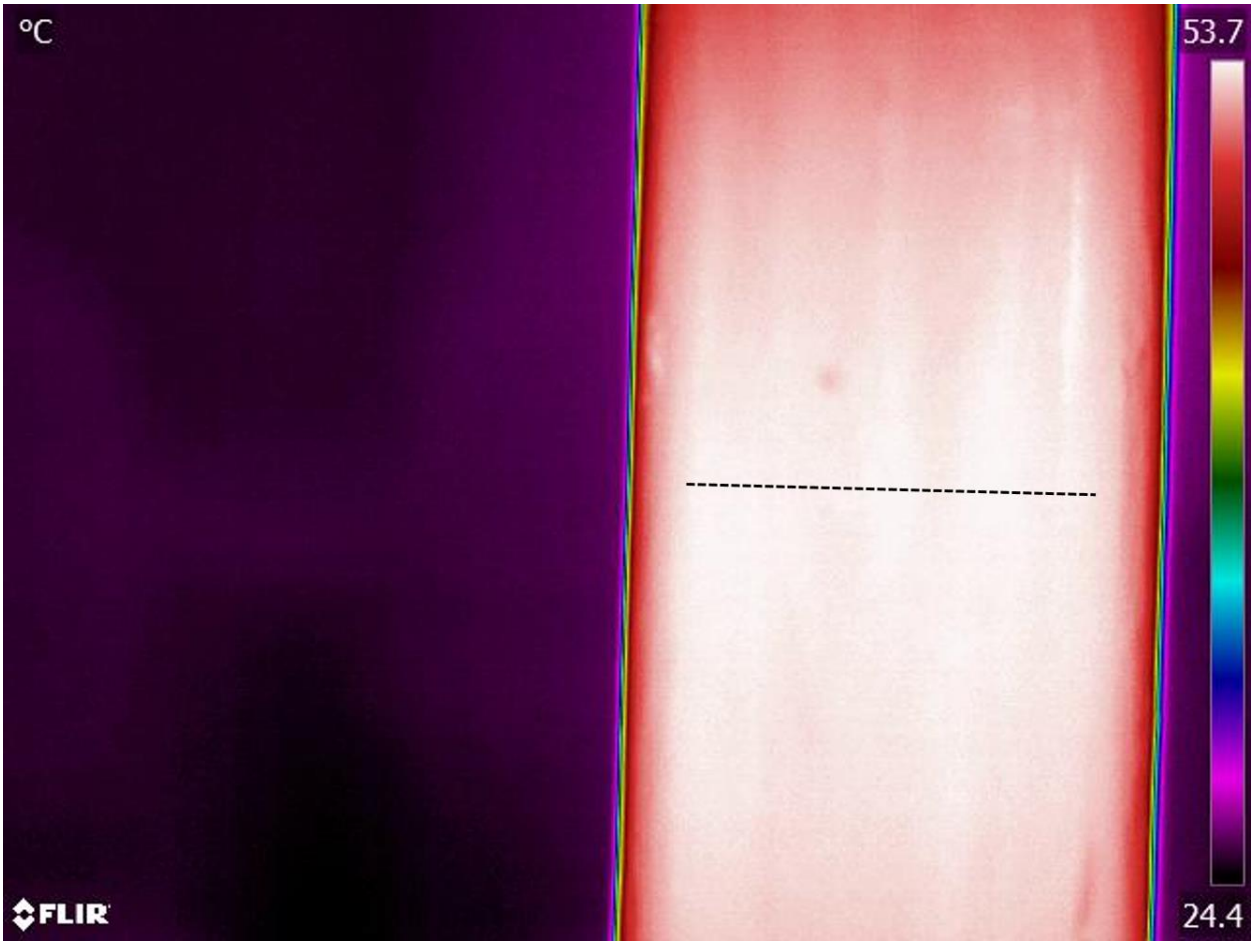

Figure 23: Effects of viewing angle on a cylindrical surface

For temperature measurements during the actual experiment the viewing angle is set to 45 ˚ with respect to stagnation point (θ=0 ˚) when viewing the front of the cylinder and is set to 45 ˚ with respect to θ=90 ˚. This is to ensure that none the temperature measurements from θ=0˚ to θ=180 ˚ are affected by the viewing angle. The IR camera is aligned to the viewing angle by aligning its resting surface with a wooden wedge which was cut had an angle of 45 ˚ between its faces.

Appendix D: IR Camera Emissivity Correction

When temperature measurements on a surface are made using an IR camera, it is desired that the emissivity of the surface is high so that accuracy of the measurements are high. For this purpose, the surface of the cylinder used in the experiments is sprayed with a uniform coating of Aervoe Z635 Black Zynolyte High Temperature Paint. Since the emissivity of the surface is unknown, a calibration procedure is required to determine its value.

D.1 Equipment Used

1. Steel Plate
2. T Type thermocouple connected to a NI9213 the thermocouple module mounted a NI cDAQ 9172 USB chassis
3. Welder to weld the thermocouple flush on the surface of the plate
4. Minco Heater with similar dimensions as the plate
5. Double sided adhesive tape to attach the heater and the plate
6. Wooden support blocks
7. DC power supply with a voltage range of 0 to 50 V and a current range of 0-1 Amp.
8. Z635 Black Zynolyte High Temperature Paint for a uniform coating black paint on the plate surface
9. FLIR A655 SC IR camera
10. Tripod for mounting the IR camera
11. Laptop to record IR and thermocouple measurement

D.2 Experimental Setup

A steel plate is painted with the same paint used on the cylinder. A beaded T type thermocouple is welded flush on the surface of the plate so to ensure that there is no air gap between the plate and the thermocouple. The other end of the thermocouple is connected to A NI DAQ which in turn is connected to a laptop. The plate is then fixed to a Minco heater of similar dimensions using double sided adhesive tape. The heater is connected to a DC power source which is capable of supplying up to 50V. The plate is then placed on a table and held upright using wooden supports for easier viewing using the IR camera.

D.3 Experimental Procedure

The heater is turned On by supplying an input voltage of 10V from the power source. The thermocouple is viewed using the IR camera and its exact location is marked on the image stream using FLIR tools. The sampling rate of the temperature readings from the thermocouple is set to 1Hz and the overall temperature of the plate is allowed to reach steady state. After this the emissivity of the IR camera is changed from 0.93-0.95 and the corresponding temperature changes are recorded. The processes repeated for 15 discreet voltage values between 10V-12 V and the thermocouple readings which are recorded using lab view 2013, are plotted against the corresponding IR camera readings. The same procedure is repeated for an input voltage range of 13-15 V and the various temperature values are compared

D.4 Calibration Results

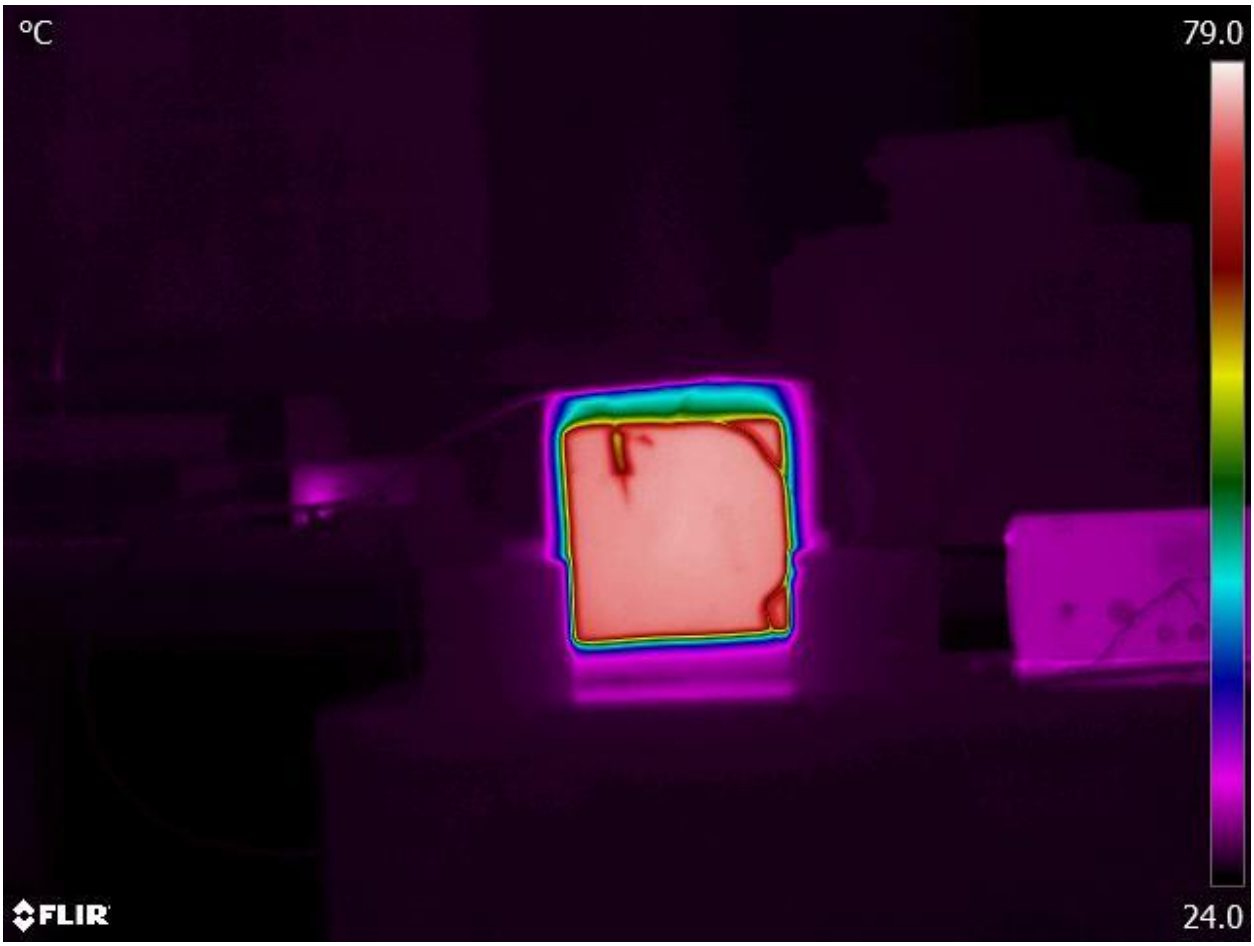

Figure 24: IR image of the flat plate used in calibration

Figure 24 shows the IR image of the steel plate used in the calibration of the IR camera. The Thermocouple is clearly visible on the top right portion of the plate. The standard error between the thermocouple and the IR camera values at emissivity of 0.93,0.94 and 0.95 are plotted. Figure 25 shows the difference in values of the thermocouple and the IR camera when the heater voltage is varied from 10-12 V

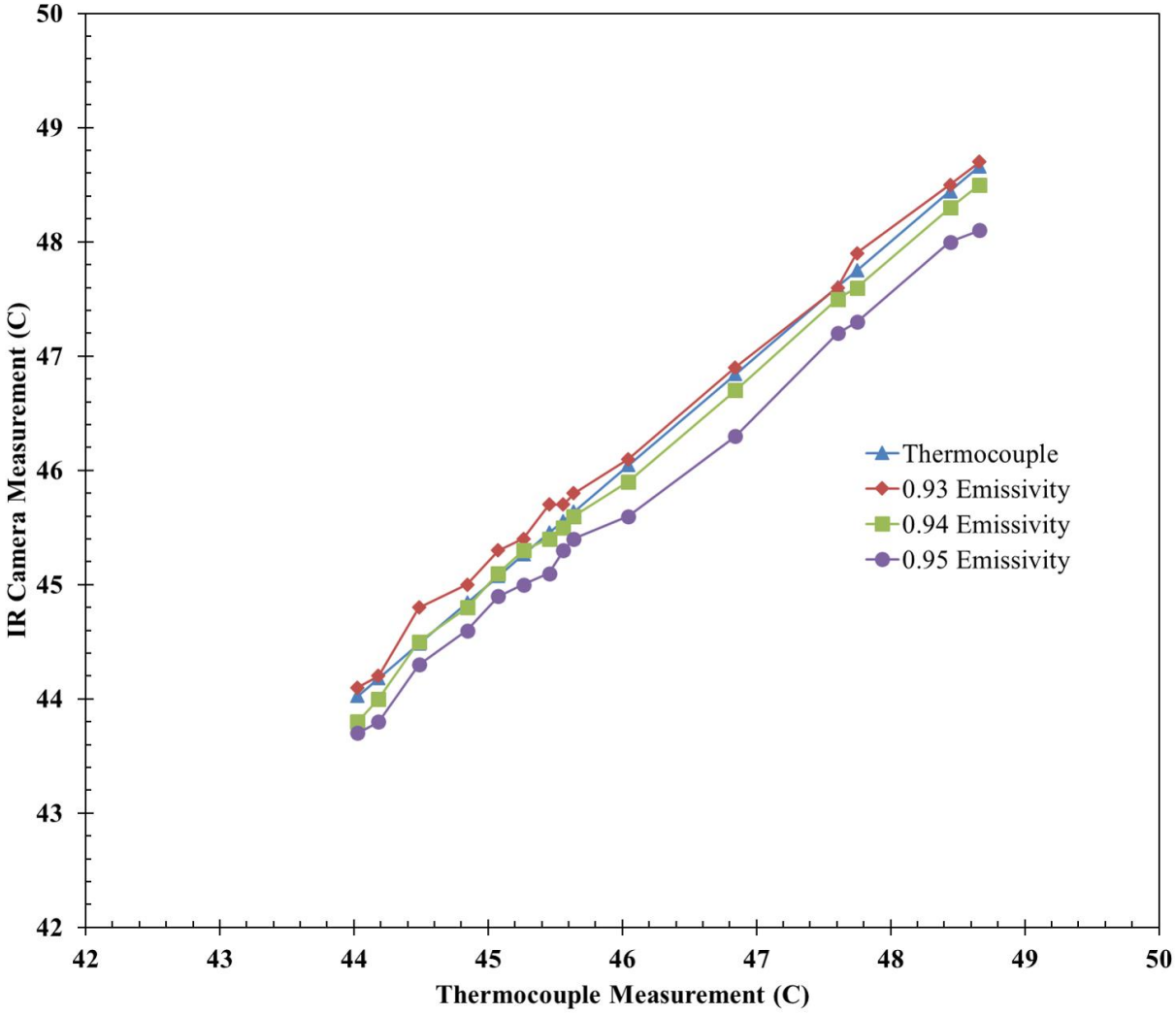

Figure 25: IR Calibration Curves at 10-12 V

The temperatures of the IR camera at emissivity of 0.94 and 0.93 had a root mean square deviation of 0.12 ˚C and 0.15 ˚C respectively from the thermocouple readings. However, when the emissivity was set at 0.95 the root mean square deviation was 0.37 ˚C. At this range of temperature an emissivity of 0.94 was chosen as the correct value.

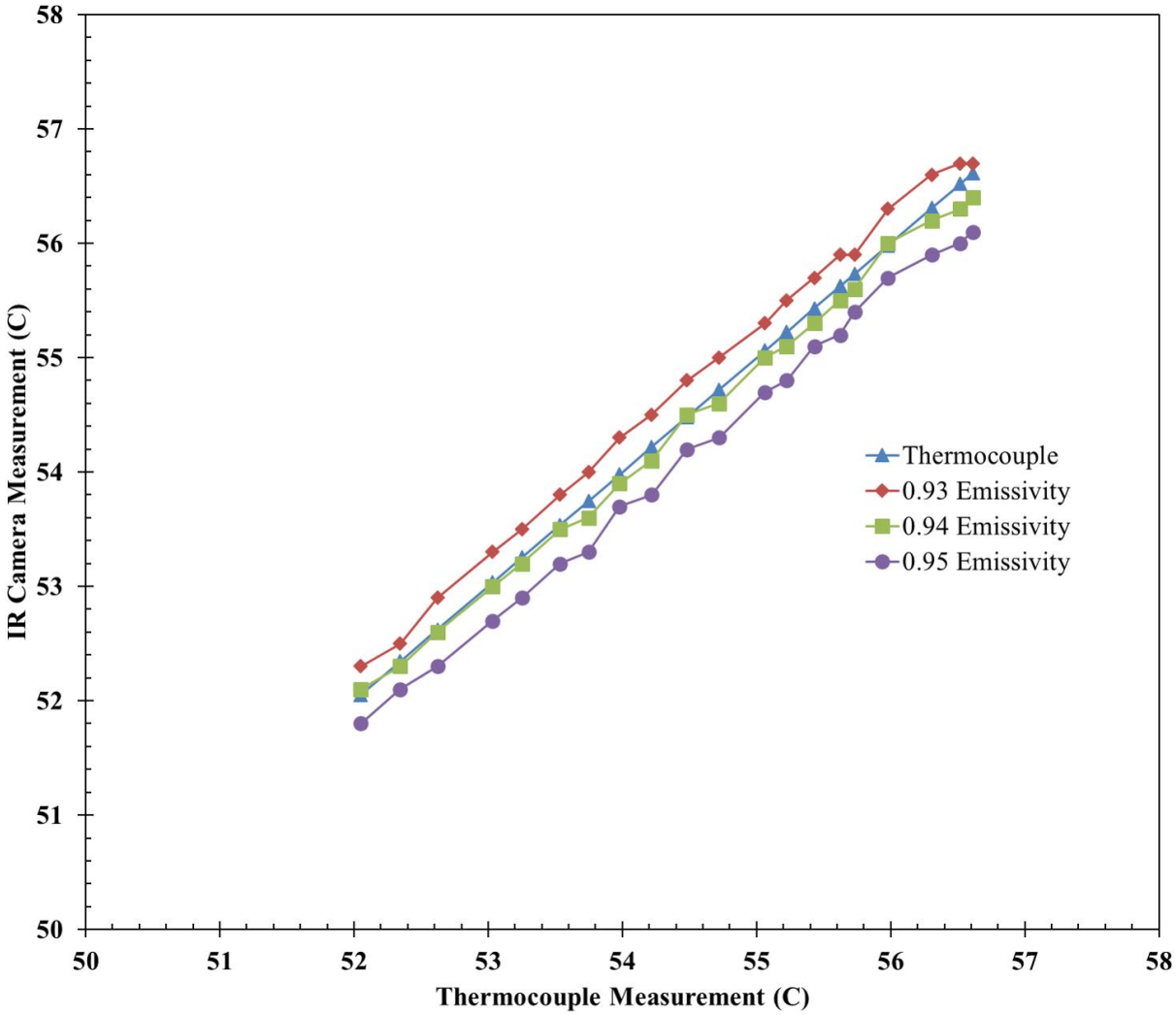

Figure 26: IR Calibration Curves at 13-15 V

Figure 26 shows the comparison of the temperature values measured by the thermocouple and the IR camera when the heater voltage is varied between at 13-15 V. The IR temperature readings of emissivity's 0.93,0.94 and 0.95 had root mean square deviations of 0.25˚C, 0.11˚C and 0.37 ˚C respectively from the thermocouple readings. The emissivity value 0.94 was the closest to the thermocouple reading at this temperate range also and hence this value was used in all experiments for the heated cylinder.